

High-resolution distributions of $\Delta(\text{O}_2/\text{Ar})$ on the northern slope of the South China Sea and estimates of net community production

Chuan Qin^{1,2}, Guiling Zhang^{1,2,*}, Wenjing Zheng¹, Yu Han^{1,3}, Sumei Liu^{1,2}

1. Key Laboratory of Marine Chemistry Theory and Technology, Ministry of Education/Institute for Advanced Ocean Study, Ocean University of China, 238 Songling Road, 266100 Qingdao, P. R. China

2. Laboratory for Marine Ecology and Environmental Science, Qingdao National Laboratory for Marine Science and Technology, Qingdao 266237, P. R. China

3. Hainan Tropical Ocean University, Sanya 572022, P. R. China

* Correspondence to: Guiling Zhang (guilingzhang@ouc.edu.cn)

Abstract

Dissolved oxygen-to-argon ratio (O_2/Ar) in the oceanic mixed layer has been widely used to estimate net community production (NCP), which is the difference between gross primary

production and community respiration and is a measure for the strength of the biological pump.

In order to obtain the high-resolution distribution of NCP and improve our understanding of its regulating factors in the slope region of the Northern South China Sea (SCS), we conducted

continuous measurements of dissolved O_2 , Ar, and CO_2 by membrane inlet mass spectrometry

(MIMS) during two cruises in October 2014 and June 2015. An overall autotrophic condition

was observed in the study region in both cruises with an average $\Delta(\text{O}_2/\text{Ar})$ of $1.1\% \pm 0.9\%$ in

October 2014 and $2.7\% \pm 2.8\%$ in June 2015. NCP was on average $11.5 \pm 8.7 \text{ mmol C m}^{-2} \text{ d}^{-1}$

in October 2014 and $11.6 \pm 12.7 \text{ mmol C m}^{-2} \text{ d}^{-1}$ in June 2015. Correlations between dissolved

inorganic nitrogen (DIN), $\Delta(\text{O}_2/\text{Ar})$, and NCP were observed in both cruises, indicating that

NCP is subject to the nitrogen limitation in the study region. In June 2015, we observed a rapid

response of the ecosystem to the episodic nutrient supply induced by eddies. Eddy-entrained

shelf water intrusion, which supplied large amounts of terrigenous nitrogen to the study region,

promoted NCP in the study region by potentially more than threefold. In addition, upwelling

brought large uncertainties to the estimation of NCP in the core region of the cold eddy (cyclone)

in June 2015. The deep euphotic depth in the SCS and the absence of correlation between NCP

and the average photosynthetically available radiation (PAR) in the mixed layer in the autumn

删除的内容: s

删除的内容: a proxy of carbon export from the surface ocean

删除的内容: 376 %

删除的内容: at

indicate that light availability may not be a significant limitation on NCP in the SCS. This study helps to understand the carbon cycle in the highly dynamic shelf system.

Keywords: O₂/Ar; Net community production; Nutrients; Eddy; Northern slope of South China Sea

1. Introduction

The oceanic carbon sequestration is partially regulated by the production and export process of biological organic carbon in the surface ocean. Net community production (NCP) corresponds to gross primary production (GPP) minus community respiration (CR) in the water (Lockwood et al., 2012) and is an important indicator of carbon export.

At steady state, NCP is equivalent to the rate of organic carbon export, and is a measure for the strength of the biological pump (Lockwood et al., 2012). NCP effectively couples carbon cycle and oxygen (O₂) production through photosynthesis and respiration in the euphotic layer, thus many previous researches measured the mass balance of O₂ to quantify NCP (e.g., Emerson et al., 1991; Hendricks et al., 2004; Huang et al., 2012; Reuer et al., 2007). Argon (Ar), a biological inert gas, was commonly used to normalize the O₂ concentration in these researches. Based on the similar solubility properties of O₂ and Ar, oxygen-to-argon ratio (O₂/Ar) can remove the influences of physical processes (i.e., temperature and pressure change, bubble injection) on the mass balance of O₂ (Craig and Hayward, 1987). Dissolved O₂/Ar has been developed as a proxy for NCP in a water mass (Kaiser et al., 2005). The biological production in the open oceans (i.e., Southern Ocean, Pacific, Arctic Ocean) has been inferred using the O₂/Ar ratio to estimate NCP in numerous researches (e.g., Hamme et al., 2012; Lockwood et al., 2012; Ulfssbo et al., 2014; Shadwick et al., 2015; Stanley et al., 2010). During recent years, several high-resolution measurements of O₂/Ar and NCP in coastal waters have been reported (Tortell et al., 2012; Tortell et al., 2014; Eveleth et al., 2017; Izett et al., 2018). Despite the coastal waters such as shelves and estuaries only accounting for 7 % of the global ocean surface area, they are known to

删除的内容: and transfer up the food web

删除的内容: hich can quantify the strength of biological pump

删除的内容: oxygen-to-argon ratio (

删除的内容:)

删除的内容: based on the similar physical properties of O₂ and Ar

删除的内容: Craig and Hayward, 1987;

contribute to 15–30 % of the total oceanic primary production (Bi et al., 2013; Cai et al., 2011) and play an important role in marine carbon cycle and production. However, these regions still suffer from low resolution measurements that can't provide representative high-resolution NCP data.

删除的内容: and

删除的内容: are poorly represented in global NCP data sets

The South China Sea (SCS) is one of the largest marginal seas in the world with complex ecological characteristics. River runoff from the Pearl and Mekong Rivers introduces large amounts of dissolved nutrients into the SCS (Ning et al., 2004). Due to the influence of seasonal monsoons, the surface circulation in the SCS changes from a basin-scale cyclonic gyre in winter to an anticyclonic gyre in summer (Hu et al., 2000). The surface water masses on the northern slope of SCS can be categorized into three regimes: shelf water, offshore water (e.g., the intruded Kuroshio water), and the SCS water (Feng, 1999; Li et al., 2018). The shelf water is mixed with fresh water from rivers or coastal currents and thus usually has low salinity ($S < 33$) and low density (Uu and Brankart, 1997; Su and Yuan, 2005; Cheng et al., 2014). Both offshore water and SCS water originate from the Northern Pacific. Thus offshore water has similar hydrographic characteristics of high temperature and high salinity as the Northern Pacific water. But the SCS water has changed a lot in its hydrographic property because of the mixing processes, heat exchange and precipitation during its long residence time of about 40 years in the SCS (Feng et al., 1999; Li et al., 2018; Su and Yuan, 2005). The distributions of phytoplankton and primary productivity of the SCS show great temporal and spatial variation (Ning et al., 2004). Low chlorophyll a (Chl a) and primary production are the significant characteristics of the SCS basin which is considered an oligotrophic region, and macronutrients (i.e. nitrogen) are the main limitations of phytoplankton growth and productivity (Ning et al., 2004; Lee Chen, 2005; Han et al., 2013). The excessive runoff from Pearl River can result in high N/P (nitrogen/phosphorus) ratio of > 100 , shifting the nutritive state from nitrogen deficiency to phosphorus deficiency in the coastal region of SCS (Lee Chen and Chen, 2006). Dissolved iron is also a potential limitation on primary production, especially in the high nutrient low chlorophyll (HNLC) regions (Cassar et al., 2011). But on the northern slope of the SCS, the concentration of dissolved iron is high enough to support

删除的内容: extremely

105 the growth of phytoplankton in the surface water (Zhang et al., 2019). The northern
106 slope of the SCS is an important transition region between coastal area and the SCS
107 basin. In the summer, the shelf water intrusion is an important process changing the
108 nutritive state in the northern slope region of the SCS (He et al., 2016; Lee Chen and
109 Chen, 2006). But so far, the NCP enhancement caused by this process is still unknown.
110 Previous studies about the organic carbon export in the SCS were mostly conducted
111 on particulate organic carbon (POC) flux (e.g., Bi et al., 2013; Cai et al., 2015; Chen et
112 al., 1998; Chen et al., 2008; Ma et al., 2008; Ma et al., 2011). Little research has been
113 conducted on NCP in the SCS to date. Chou et al. (2006) estimated NCP in the northern
114 SCS during the summertime to be $4.47 \text{ mmol C m}^{-2} \text{ d}^{-1}$ based on the time change rate
115 of dissolved inorganic carbon (DIC) in the mixed layer at the South East Asia Time-
116 Series Station (SEATS) from 2002 to 2004. Wang et al. (2014) used GPP and CR data
117 from a light/dark bottle incubation experiment to calculate NCP in the northern SCS
118 and obtained a range from -179.0 to $377.6 \text{ mmol O}_2 \text{ m}^{-2} \text{ d}^{-1}$ (-129.7 to 273.6 mmol C
119 $\text{m}^{-2} \text{ d}^{-1}$). Huang et al. (2018) estimated monthly NCP from July 2014 to July 2015 based
120 on in situ O_2 measurements on an Argo profiling float and reported the cumulative NCP
121 to be $0.29 \text{ mol C m}^{-2} \text{ month}^{-1}$ ($9.67 \text{ mmol C m}^{-2} \text{ d}^{-1}$) during the northeast monsoon
122 period and $0.17 \text{ mol C m}^{-2} \text{ month}^{-1}$ ($5.67 \text{ mmol C m}^{-2} \text{ d}^{-1}$) during the southwest
123 monsoon period in the SCS basin. However, most of these studies in the SCS were
124 constrained by methodological factors attributed to discrete sampling and cannot reveal
125 the rapid productivity response to highly dynamic environmental fluctuations of coastal
126 systems. Discrete sampling suffers from low spatial resolution, and cannot adequately
127 resolve variabilities caused by small-scale physical or biological processes in the
128 dynamic marine systems. In addition, each of the three methods for NCP estimate
129 mentioned above has its limitation. DIC-based NCP estimate is not suitable for the
130 coastal region, because instead of biological metabolism, the terrestrial runoff can be
131 the strongest factor influencing the DIC in the coastal system (Mathis et al., 2011). The
132 inavoidable difference between in situ circumstance and on-deck incubation condition
133 can introduce uncertainties to the NCP derived from light/dark bottle incubation
134 (Grande et al., 1989). Though Argo profiling float partly gets rid of the limitation of

删除的内容: community respiration

discrete sampling, it's hard to control its movement in the study region. However, no high-resolution measurement of NCP has been reported for the SCS so far.

In this paper, we present high-resolution NCP estimates in the northern slope region of the SCS based on continuous shipboard dissolved O₂/Ar measurement. We discuss the regulating factors of NCP based on ancillary measurements of other hydrographic parameters. Our high-resolution measurements caught the rapid response of the ecosystem to the episodic nutrient supply induced by eddies and help us to quantify the contribution of eddy-entrained shelf water intrusion to NCP in the summer cruise.

2. Methods

2.1 Continuous underway sampling and measurement

Continuous measurements of dissolved gases (O₂, Ar, and CO₂) were obtained using membrane inlet mass spectrometry (MIMS, HPR 40, Hiden Analytical, UK) (Tortell, 2005) onboard the *R/V 'Nanfeng'* during two cruises in the northern slope region of the SCS (Figures 1a, 1b) from 13 to 23 October 2014 and from 13 to 29 June 2015. In addition, a cyclonic-anticyclonic eddy pair was observed in June 2015 (Figure 1c) and resulted in dramatic influences on the study region.

We developed a continuous shipboard measurement system of dissolved gases following the method described by Guéguen and Tortell (2008). Surface seawater was collected continuously using the ship's underway intake system (~5 m depth) and was divided into different lines for various underway scientific measurements. Seawater from the first line passed through a chamber at a flowrate of 2–3 L min⁻¹ to remove macroscopic bubbles and to avoid pressure bursts. A flow of ~220 mL min⁻¹ was continuously pumped from the chamber using a Masterflex Peristaltic Pump equipped with L/S® multichannel cartridge pump heads (Cole Parmer). In order to minimize the O₂/Ar fluctuations due to temperature effects and water vapor pressure variations, the water samples flowed through a stainless steel coil (~6 m) with 0.6 mm wall thickness immersed in a water bath (Shanghai Bilon Instrument Co. Ltd, China) to achieve a constant temperature (~2 °C below the sea surface temperature), which avoided

删除的内容: outh China Sea

删除的内容: s

删除的内容: outh China Sea

168 temperature-induced supersaturation and subsequent bubble formation. Then the water
169 samples were introduced into a cuvette with a silicone membrane mounted on the inside.
170 The analyte gases were monitored by a Faraday cup detector in the vacuum chamber
171 after diffusion through the silicone membrane, and the signal intensities at the relevant
172 mass to charge (m/z) ratios (32, 40 and 44 for O₂, Ar and CO₂, respectively) were
173 recorded by MASSoft. Based on the continuous measurement of 50 L air-equilibrated
174 seawater, the long-term signal stability (measured as the coefficient of variation) over
175 12 h was 1.57 %, 3.75 % and 2.21 % for O₂, Ar and CO₂, respectively. Seawater from
176 the second line passed through a flow chamber, where an RBR Maestro (RBR, Canada)
177 was installed to continuously record temperature, salinity, dissolved oxygen (DO), and
178 Chl a. We didn't obtain continuous DO data in October 2014 because the DO sensor of
179 RBR broke down. A third line was used to drain the excess seawater. Underway
180 pipelines were flushed with freshwater or bleach every day, to avoid possible in-lines
181 biofouling. The data from the underway transects were exported to spreadsheets and
182 compiled into 5 min averages, and the comparisons of the gas data with other
183 hydrographic variables were based on the UTC time recorded for each measurement.

184 The O₂/Ar ratio measurements were calibrated with air-equilibrated seawater samples
185 at about 6–8 h intervals to monitor instrument drift and calculate $\Delta(\text{O}_2/\text{Ar})$. These air-
186 equilibrated seawater samples were prefiltered (0.22 μm) and bubbled with ambient air
187 for at least 24 h to reach equilibrium at sea surface temperature (Guéguen and Tortell,
188 2008). For calibration, 800 mL of air-equilibrated seawater sample was transferred into
189 glass bottles and immediately drawn into the cuvette, where the first 200 mL of the
190 sample was used to flush the cuvette and pipelines. After 3 min recirculation of the
191 sample, the average signal intensity was obtained to calculate O₂/Ar. During the course
192 of measurements, flow rate and the temperature of water bath were both kept the same
193 as the underway measurements. The precision of MIMS-measured O₂/Ar was 0.22 %,
194 based on analyses of 20 duplicate samples in the laboratory test, which is comparable
195 to previous studies and sufficient to detect biologically driven gas fluctuations in
196 seawater (Tortell, 2005).

197 The instrumental CO₂ ion current was calibrated at about 12–24 h intervals using

删除的内容: during this cruise

equilibrated seawater standards as per Guéguen and Tortell (2008) during the survey in June 2015. Prefiltered seawater (0.22 µm) was gently bubbled with dry CO₂ standards (200, 400, and 800 ppm, provided by the Chinese National Institute of Metrology) at in situ temperature. After 2 days of equilibrium, these standards were analyzed by MIMS following the same procedure for measuring air-equilibrated seawater samples to obtain a calibration curve between CO₂ signal intensity and mole fraction. The reproducibility of these measurements was better than 5 % within 15 days. Then we used the empirical equations reported by Takahashi et al. (2009) to convert the CO₂ mole fraction derived from the calibration curve to the in situ partial pressure of CO₂ (*p*CO₂).

Chlorophyll-a (Chl a) data from the RBR sensor were linear calibrated against extracted Chl a measurements of discrete seawater samples taken from the same seawater outlet as for MIMS measurements. Samples were filtered through polycarbonate filters (0.22 µm). The filter membranes were then packed with pre-sterilized aluminum foil and stored in a freezer (−20 °C) until extraction by acetone and analysis using a fluorimetric method (F-4500, HITACHI, Japan) described by Parsons (1984). The mean residual of this calibration was 0.00 ± 0.07 µg L^{−1}.

2.2 Estimation of NCP based on O₂/Ar measurements

NCP in the mixed layer was estimated by the O₂/Ar mass balance from continuous measurements. Due to similar physical properties of O₂ and Ar, Δ(O₂/Ar) is used as a proxy of the biological O₂ supersaturation and is defined as (Craig and Hayward, 1987):

$$\Delta(O_2 / Ar) = \frac{([O_2]/[Ar])}{([O_2]/[Ar])_{eq}} - 1$$

where [O₂]/[Ar] is the measured dissolved O₂/Ar ratio of the mixed layer and ([O₂]/[Ar])_{eq} is the measured dissolved O₂/Ar ratio of the air-equilibrated seawater samples. Δ(O₂/Ar) is the percent deviation of the measured O₂/Ar ratio from the equilibrium. Assuming a steady state and negligible physical supply, NCP is the air–sea biological O₂ flux and can be estimated as (Reuer et al., 2007):

$$NCP (mmol C m^{-2} d^{-1}) \approx k_{O_2} \cdot [O_2]_{sat} \cdot \Delta(O_2 / Ar) \cdot r_{C:O_2} \cdot \rho$$

where k_{O_2} is the weighted gas transfer velocity of O₂ (m d^{−1}); [O₂]_{sat} denotes the

228 saturation concentration of dissolved O_2 ($\mu\text{mol kg}^{-1}$) in the mixed layer, which is
 229 calculated based on temperature and salinity (Weiss, 1970); $r_{C:O_2}$ is the photosynthetic
 230 quotient of C and O_2 and was reported as 1:1.38 in the SCS (Jiang et al., 2011); ρ is
 231 seawater density in units of kg m^{-3} (Millero and Poisson, 1981). We estimated k_{O_2}
 232 using the European Centre for Medium-Range Weather Forecasts (ECWMF) wind-
 233 speed reanalysis data product with a $0.25^\circ \times 0.25^\circ$ grid (<https://www.ecmwf.int>), the
 234 parameterization by Wanninkhof (1992), and the gas exchange weighting algorithm by
 235 Teeter et al. (2018). Teeter et al., (2018) pointed out that modern O_2/Ar method does
 236 not strongly rely on the steady state assumption. When this assumption is violated, our
 237 estimate does not represent the actual daily NCP but rather an estimate of NCP
 238 weighted over the residence time of O_2 in the mixed layer and along the path of the
 239 water parcel during that period. Thus the residence time of O_2 in the mixed layer is an
 240 important implication of the weighted timescale of NCP before the measurement of
 241 O_2/Ar . The residence time of O_2 (τ , d) in the mixed layer is estimated as the ratio of
 242 mixed layer depth (MLD, m) to the gas transfer velocity of O_2 (k_{O_2} , m d^{-1}) (Jonsson
 243 et al., 2013).

244 245 **2.3 Ancillary measurements and calculations**

246 Surface water samples for the nutrient analysis were collected from Niskin bottles
 247 mounted on the CTD, where the samples were filtered through acid-cleaned acetate
 248 cellulose filters (pore size: $0.4 \mu\text{m}$). The filtrates were poisoned by HgCl_2 and stored in
 249 the dark at 4°C . In the laboratory, the nutrients were determined photometrically by an
 250 auto-analyzer (QuAatro, SEAL Analytical, Germany) with a precision better than 3 %.
 251 MLD, was defined by the $\Delta\sigma_t = 0.125 \text{ kg m}^{-3}$ criterion (Monterey and Levitus, 1997).
 252 The subsurface chlorophyll maximum layer (SCML) was observed using the
 253 fluorescence sensor mounted on the CTD. SCML usually occurs at the bottom of
 254 euphotic layer (Hanson et al., 2007; Liao et al., 2018; Teira et al., 2005). Because no
 255 PAR (Photosynthetically Available Radiation) data were obtained in two cruises, we
 256 decided to regard the depth of SCML as the euphotic depth (Z_{eu}). Both MLD, and Z_{eu}
 257 were calculated at each station, where the vertical CTD casts were made. The MLDs for

删除的内容: The

删除的内容: s

删除的内容: were

删除的内容: ,

删除的内容: and it

删除的内容: The

删除的内容: s

删除的内容: the SCML

删除的内容: the

删除的内容: s

underway data between CTD stations was calculated using linear interpolation based on the distance between the underway points and nearest CTD stations. We matched the underway data to each CTD location using a combination of latitude/longitude threshold (latitude/longitude of CTD station $\pm 0.05^\circ$) and time threshold (end/start of stationary time ± 1 h), then took the averages of these underway data for further analysis with discrete nutrient concentrations.

The daily satellite chlorophyll data were obtained from [the E.U. Copernicus Marine Service Information](https://resources.marine.copernicus.eu) website (<https://resources.marine.copernicus.eu>). The product we used was provided by ACRI-ST company (Sophia Antipolis, France), with a space-time interpolation (the “Cloud Free”). [The M_Map package for Matlab was applied to output satellite chlorophyll images \(Pawlowicz, 2020\)](#). Daily and 8-day PAR data collected by MODIS-Aqua sensor were obtained from NASA’s ocean color website (<https://oceancolor.gsfc.nasa.gov/13>). The spatial resolution of both satellite products is 4 km, and we match the satellite PAR with CTD location by choosing the closest PAR data point to the CTD location. A light attenuation coefficient (K_d , m^{-1}) was used to estimate the average PAR in the mixed layer (Kirk 1994; Jerlov 1976):

$$K_d = \frac{4.605}{Z_{eu}}$$

3. Results and Discussion

3.1 Distributions of hydrographic parameters and gases

The distributions of temperature, salinity, Chl a, and $\Delta(O_2/Ar)$ during the autumn cruise (October 2014) are shown in Figure 2. Sea surface temperature (SST) ranged from 26.96 °C to 28.53 °C with an average of 27.82 ± 0.33 °C. Sea surface salinity (SSS) ranged from 33.28 to 34.11 with the low values occurring in the southeast of the region. Chl a concentration ranged from 0.01 to 0.71 $\mu g L^{-1}$ and was in an average of 0.18 ± 0.13 $\mu g L^{-1}$, which was comparable to the 11-year mean value (~ 0.2 $mg m^{-3}$) in the same region in October reported by Liu et al. (2014). $\Delta(O_2/Ar)$ values were in the range of -2.9 – 4.9 % (avg. 1.1 % ± 0.9 %) and [slightly oversaturated in most areas](#) (Figure 2d). [Please note that all averages we have published in this paper are reported in the](#)

删除的内容: the Copernicus

删除的内容: most areas were

删除的内容: In addition, p

format of *mean ± standard deviation*.

In June 2015, SST ranged from 29.28 °C to 32.24 °C and was in an average of 30.88 ± 0.59 °C (Figure 3a). SSS ranged from 30.81 to 34.16. Transect 3 was significantly characterized by low salinity (Figure 3b). He et al (2016) reported that this phenomenon was influenced by the eddy-entrained Pearl River plume (shelf water) injected into the SCS. Chl a varied in a range of 0.09–0.58 µg L⁻¹ in the study region. Under the influence of this **eddy-entrained shelf** water, Chl a values higher than 0.30 µg L⁻¹ were observed along Transect 3 (Figure 3c). In contrast, Chl a was in the range of 0.09–0.18 µg L⁻¹ along Transect 1 and 2. It was obvious that DO was much higher in the east side than the west side in the study region (Figure 3d). Δ(O₂/Ar) ranged from -3.9–13.6 %. Most of the Δ(O₂/Ar) values were positive in the study region (avg. 2.7 % ± 2.8 %), whereas the negative values were concentrated along Transect 4 (Figure 3f). Δ(O₂/Ar) along Transect 3 was in an average of 7.2 % ± 2.6 %, significantly higher than that of other transects (Figure 3f). *p*CO₂ exhibited a high degree of spatial and temporal variability and the high values mostly occurred on the west side of the study region (Figure 3e). Resulting from the considerable low *p*CO₂ in Transect 3, the average *p*CO₂ (323 ± 93 µatm) in the study region was lower than those reported previously, i.e., 350–370 µatm by Zhai et al (2009) and 340–350 µatm by Rehder and Sues (2001). Due to the influence of the **shelf** water, the average *p*CO₂ in Transect 3 was 222 ± 33 µatm, with a range of 144–321 µatm. In the summer, shelf water mixed with Pearl River plume is the most important factor influencing *p*CO₂ in the coastal and shelf region of **the** northern SCS, which can result in the *p*CO₂ values as low as 150 µatm (Li et al., 2020). Here we apply an average atmospheric *p*CO₂ of 382 µatm that observed in July 2015 in the northern SCS (Li et al., 2020) to calculate the *p*CO₂ difference (Δ*p*CO₂) between the surface water and the atmosphere. Δ*p*CO₂ ranged from -238 to -61 µatm along Transect 3, indicative of a strong CO₂ sink.

3.2 Mixed layer depth, euphotic depth and residence time of O₂ in the mixed layer

MLD, euphotic depth (*Z*_{eu}) and the residence time of O₂ (τ) in the mixed layer at CTD stations of two cruises are shown in Table 1 and 2. In autumn 2014, MLD ranged from

删除的内容:),

删除的内容: respectively

27 to 81 m, with an average of 55 ± 15 m (Table 1). The average Z_{eu} was 74 ± 12 m, approximately 20 m deeper than MLD (Table 1). The residence time of O_2 in the mixed layer ranged from 3 to 13 d (Table 1), comparable to a range of 1–2 weeks reported by previous studies (Izett et al., 2018; Manning et al., 2017). The average residence time of O_2 was 9 ± 3 d, indicating that our estimate generally quantified NCP over 9 days prior to the underway observation of O_2/Ar during this cruise.

删除的内容: reasonable

删除的内容: in the mixed layer

The average MLD in June 2015 was just 18 ± 6 m (Table 2). Significant shallow MLD occurred at two stations (J-10, J-11) located in Transect 3 (Table 2, Figure S1f). The low-salinity shelf water intrusion is the main cause of this shallow MLD of 8 m. The average Z_{eu} was 58 ± 18 m, approximately 40 m deeper than MLD (Table 2). The residence time of O_2 in the mixed layer ranged from 2 to 12 d (Table 2), indicating a fast gas exchange in some stations. In addition, we also observed relatively obvious subsurface O_2 maxima in Transect 1 and 2 in summer 2015. But this phenomenon didn't exist in autumn 2014.

删除的内容: , shallower than that of October 2014

In both cruises, Z_{eu} was observed obviously deeper than MLD. This result partly suggests that light availability may not be a limitation of NCP in the northern slope of SCS. Especially in the summer, Z_{eu} extended to 2–7 times of MLD (Table 2), ensuring sufficient illumination in the mixed layer. But in the autumn when the thickness of mixed layer accounts for about 74 % of euphotic layer, the average light intensity in the mixed layer might be influenced by the exponentially light attenuation along depth.

3.3 NCP in autumn and summer

In October 2014, NCP in the northern slope of the SCS ranged from -29.2 to 42.7 mmol $C\ m^{-2}\ d^{-1}$ (avg. 11.5 ± 8.7 mmol $C\ m^{-2}\ d^{-1}$) and most of the region was net autotrophic (Figure 4a). The estimated NCP based on the O_2/Ar values measured in this cruise is about 34 % of the net primary production rates of 34.3 mmol $C\ m^{-2}\ d^{-1}$ measured by ^{14}C bottle incubation (Sun X., personal communication), which was in agreement with previous research (Quay et al., 2010).

The average NCP in the study region was 11.6 ± 12.7 mmol $C\ m^{-2}\ d^{-1}$ with a range of -27.6 – 61.4 mmol $C\ m^{-2}\ d^{-1}$ in June 2015. A high NCP level was observed along

Transect 3 (Figure 4b). Eddy-entrained shelf water brought a large amount of terrigenous nutrients from the shelf to the slope region along Transect 3 (He et al., 2016). The average nitrate (NO_3^-) and nitrite (NO_2^-) concentrations in the surface water of Transect 3 were $2.31 \pm 0.70 \mu\text{mol L}^{-1}$ and $0.04 \pm 0.01 \mu\text{mol L}^{-1}$ respectively (Figure S1a, S1b); both values were much higher than those found in the other three transects where NO_3^- was in a range of < 0.03 – $0.69 \mu\text{mol L}^{-1}$ and NO_2^- was mostly below the detection limit. Li et al. (2018) reported that the entire Transect 3 and part of Transect 4 were dominated by shelf water at the surface and we estimated NCP over these regions where salinity lower than 33 as $23.8 \pm 10.7 \text{ mmol C m}^{-2} \text{ d}^{-1}$ on average. We also observed a warm eddy (anti-cyclone) covering most stations in Transects 1 and 2 (Figure 1b, 1c) during our survey in June 2015 (Chen et al., 2016). Anti-cyclonic eddies can cause downwelling, deepening of the thermocline, and blocking of the supply of nutrients from the deeper water (Ning et al., 2008; Shi et al., 2014). Consequently, a warm eddy is expected to result in an oligotrophic condition in the surface water associated with low Chl a concentrations and low production (Ning et al., 2004). As a result, in the summer of 2015, the observed NO_2^- , NO_3^- , and PO_4^{3-} (phosphate) concentrations were almost below the detection limit in Transects 1 and 2 (Figure S1a, S1b, S1d). NCP in Transect 1 and 2 was at a very low level (avg. $2.8 \pm 2.7 \text{ mmol C m}^{-2} \text{ d}^{-1}$). Because of the significant high values of NCP over the regions with shelf water intrusion, our NCP result in the summer of 2015 is averagely higher than the previous values of $4.47 \text{ mmol C m}^{-2} \text{ d}^{-1}$ and $0.17 \text{ mol C m}^{-2} \text{ month}^{-1}$ ($5.67 \text{ mmol C m}^{-2} \text{ d}^{-1}$) based on DIC budget and Argo- O_2 respectively in the SCS (Chou et al., 2006; Huang et al., 2018). However, NCP estimates based on both methods mentioned above suffer from poor temporal and spatial coverage and do not allow for revealing rapid changes in shelf systems. In contrast, continuous measurements of O_2/Ar allow us to capture rapid variations in NCP along Transect 3 and resolve short-term productivity responses to environmental fluctuations.

3.4 Distribution of various parameters along representative transects

We chose Transect 5 (Figure 1a) observed in October 2014 and Transect 4 (Figure 1b)

394 observed in June 2015 to show the distribution of various parameters.

395 The distribution of Chl a, $\Delta(\text{O}_2/\text{Ar})$, and NCP showed similar trend along Transect 5
396 in October 2014 (Figure 5). There ~~was a trough of temperature, showing a maximum~~
397 drawdown of $\sim 0.6^\circ\text{C}$ compared to the average temperature in the study region (Figure
398 5a). But the temperature fluctuations shown here are too small to reflect a significant
399 upwelling that can easily cause $\sim 2^\circ\text{C}$ drawdown of temperature in the upper layer (Lin
400 et al., 2013; Manning et al., 2017; Ning et al., 2004). A spike of Chl a occurred between
401 115.6°E and 115.7°E and was coincident with the peaks of $\Delta(\text{O}_2/\text{Ar})$ and NCP (Figure
402 5b, 5c). The highest surface concentration of ammonium (NH_4^+) of $0.35\ \mu\text{mol L}^{-1}$ was
403 also observed between 115.6°E and 115.7°E in this transect and was predominantly
404 higher than the concentrations ($0.07\text{--}0.17\ \mu\text{mol L}^{-1}$) in the other regions of this cruise
405 (Figure 5c, S2b). Because no significant obduction processes (i.e., upwelling,
406 entrainment, and diapycnal mixing) were reported in this region, the most likely source
407 of this abundant NH_4^+ was in situ regeneration ~~such as the~~ excretion of zooplankton and
408 the bacterial decomposition of organic matter (La Roche, 1983; Clark et al., 2008).
409 ~~Theoretically, NH_4^+ , an important nitrogen source of phytoplankton growth, can be~~
410 quickly utilized by phytoplankton, and contributes to primary production (Dugdale and
411 Goering, 1967; Tamminen, 1982). ~~However, we only got nutrient data at two CTD~~
412 stations in this transect, ~~thus the result we obtained here just indicated that high NCP~~
413 ~~occurred at the station with relatively high NH_4^+ concentration, but couldn't be a strong~~
414 ~~evidence that NH_4^+ was the main factor influencing NCP in this transect.~~

415 A similar distribution pattern of Chl a, NCP, and $\Delta(\text{O}_2/\text{Ar})$ was observed along
416 Transect 4 in June 2015, whereas $p\text{CO}_2$ showed the opposite trend for these three
417 parameters (Figure 6b, 6c). Low salinity (lower than 33) existed at both southern and
418 northern ends of this transect (Figure 6a). The concentration of dissolved inorganic
419 nitrogen (DIN , $\text{NO}_3^- + \text{NO}_2^- + \text{NH}_4^+$) in the surface water was $0.81\ \mu\text{mol L}^{-1}$ and 0.27
420 $\mu\text{mol L}^{-1}$ at the southern and northern end respectively, which was higher than the
421 concentrations in other stations of this transect (Figure 6c). These results indicate that
422 shelf water is imported at the northern and southern ends of this transect, along with
423 higher levels of Chl a and NCP (Figure 6c). A sharp drop in the temperature and an

删除的内容: 's

删除的内容: were considered to be the main mechanisms for the release of NH_4^+ into the surface water

删除的内容: Ammonium

删除的内容: is

删除的内容: which

删除的内容: Though

删除的内容: partly indicated that higher ammonium could result in higher $\Delta(\text{O}_2/\text{Ar})$ and NCP.

increase in salinity occurred from 19.7°N to 19.8°N and from 21°N to 20.7°N (Figure 6a), manifesting an upwelling over this area together with dramatic spikes in $p\text{CO}_2$ and associated decrease in $\Delta(\text{O}_2/\text{Ar})$ (Nemcek et al., 2008) (Figure 6b). Most regions of Transect 4 were dominated by upwelling and showed negative sea level height anomaly (Chen et al., 2016; He et al., 2016). A localized cold eddy was considered the cause of this upwelling (Figure 1c), resulting in a maximum temperature drawdown of $\sim 1.6^\circ\text{C}$ in the mixed layer.

Vertical mixing is considered the largest source of error in O_2/Ar -based NCP estimates because the upwelled subsurface water with different O_2/Ar signatures can produce either an overestimation or an underestimation of NCP in the mixed layer (Cassar et al., 2014; Izett et al., 2018). Former researches usually ignored the underestimated negative NCP that caused by vertical mixing (Giesbrecht et al., 2012; Reuer et al., 2007; Stanley et al., 2010). Cassar et al. (2014) presented a N_2O -based correction method of O_2/Ar and NCP for vertical mixing. Although this method has been successfully adopted by Izett et al. (2018) in the Subarctic Northeast Pacific, it is not suitable for our study region. This is because it is basically applicable in the areas where the depths of euphotic zone and mixed layer are similar, and this method is not suitable for oligotrophic regions (Cassar et al., 2014). The SCS is recognized as an oligotrophic region and the depth of the euphotic zone can be 2–7 times that of the mixed layer in our study region in the summer. In addition, in the region (e.g. the SCS basin) where subsurface oxygen maximum exists, the applicability of N_2O -based correction method is limited (Izett et al., 2018). In Transect 4, the regions with negative NCP and the regions with salinity higher than 33.5 and temperature lower than 30°C are defined as influenced by upwelling. If we neglect these regions in Transect 4, the average NCP in June 2015 can slightly raise to $12.4 \pm 12.3 \text{ mmol C m}^{-2} \text{ d}^{-1}$. If we also remove the influence of shelf water intrusion by neglecting the regions with salinity lower than 33, the average NCP can sharply decrease to $5.0 \pm 6.2 \text{ mmol C m}^{-2} \text{ d}^{-1}$, which was similar to the results of $4.47 \text{ mmol C m}^{-2} \text{ d}^{-1}$ and $0.17 \text{ mol C m}^{-2} \text{ month}^{-1}$ ($5.67 \text{ mmol C m}^{-2} \text{ d}^{-1}$) reported in previous researches in the same season (Chou et al., 2006; Huang et al., 2018). Here we regard $5.0 \pm 6.2 \text{ mmol C m}^{-2} \text{ d}^{-1}$ as the background value of NCP in the

study region. Since an average NCP of $23.8 \pm 10.7 \text{ mmol C m}^{-2} \text{ d}^{-1}$ was observed over the regions with salinity lower than 33, we can conclude that the summer shelf water intrusion significantly promoted NCP by potentially more than threefold in June 2015.

删除的内容: about 376 %

3.5 Factors influencing NCP in the SCS

The SCS is an oligotrophic region with low biomass and primary production (Lee Chen, 2005; Ning et al., 2004). Previous research has shown that the nutrient, especially nitrogen and phosphorus, is the most important factor controlling and limiting the phytoplankton biomass and primary production in the SCS (Ning et al., 2004; Lee Chen, 2005; Lee Chen and Chen, 2006; Han et al., 2013). After neglecting the two CTD stations (J-14, J-15) with negative NCP influenced by upwelling in June 2015, we performed a principal component analysis (PCA) to determine the dominant factors influencing NCP in both cruises. In October 2014, DIN (0.741), $\Delta(\text{O}_2/\text{Ar})$ (0.858), and NCP (0.979) were significantly loaded on Factor 1, indicating a potential relationship among these three variables (Figure 7a, Table S1b). The correlation coefficient between DIN and NCP was 0.706 ($p < 0.01$, Table S1a), which was significantly higher than the coefficient between NCP and the other variables, except for $\Delta(\text{O}_2/\text{Ar})$ and temperature; this indicated that DIN was an important factor influencing NCP in this cruise. Another two nutrients – dissolved silicate (DSi , SiO_3^{2-}) and dissolved inorganic phosphorus (DIP , PO_4^{3-}) – had no correlations ($p > 0.05$) with NCP (Table S1a). In June 2015, Factor 1 showed a strong loading by DIN (0.876), Chl a (0.950), DO (0.927), $\Delta(\text{O}_2/\text{Ar})$ (0.902), and NCP (0.909), whereas salinity (−0.936) and $p\text{CO}_2$ (−0.908) were negatively loaded on Factor 1 (Figure 7b, Table S2b). The injection of low salinity shelf water appeared to have a strong effect on the study region because significant negative correlations were observed between salinity and DIN, Chl a, $\Delta(\text{O}_2/\text{Ar})$, and NCP (Table S2a). DIN had strong correlations with NCP, $\Delta(\text{O}_2/\text{Ar})$, and Chl a, with the correlation coefficients of 0.747, 0.910, and 0.754, respectively (Table S2a), indicating that DIN was the dominant factor controlling the growth of phytoplankton and primary production in this cruise. DSi (0.582) and DIP (−0.601) were both moderately loaded on Factor 2 (Figure 7b, Table S2b) and had no correlations with NCP ($p > 0.05$, Table

S2a). These results suggested the key role of nitrogen in regulating $\Delta(\text{O}_2/\text{Ar})$, NCP, and phytoplankton biomass in the SCS. The supply of nitrogen may stimulate the growth of phytoplankton in the SCS and nitrogen is an important participant in photosynthesis and a basic element that contributes to the increase in primary production (Dugdale and Goering, 1967; Lee Chen, 2005; Lee Chen and Chen, 2006; Han et al., 2013).

Coupled with biochemical variations, physical processes also play important roles in the slope region of the SCS by transporting abundant nutrient-rich shelf water into the SCS and bringing deep water to the surface by enhancing water mixing (Chen and Tang, 2012; Ning et al., 2004; Pan et al., 2012). The surface waters in the slope region of the northern SCS are primarily composed of waters originating from SCS water, Kuroshio water, and shelf water (Li et al., 2018). In the summer, the shelf water exists where the potential density anomaly is lower than 20.5 kg m^{-3} (Li et al., 2018). In the autumn, there is a weak offshore transport of the shelf water in the SCS and the salinity of the water mixed with the shelf water is usually lower than 33 (Fan et al., 1988; Uu and Brankart, 1997; Su and Yuan, 2005). In October 2014, the observed surface salinity was in a range of 33.28 to 34.11; thus the surface waters were mainly derived from mixing of the Kuroshio water and the SCS water. In the summer of 2015, a cyclonic-anticyclonic eddy pair was observed in the study region (Figure 1c). Low-salinity shelf water mixed with the intruding river plume from the Pearl River in the upper 50 m and was transported to the slope and basin along the intersection of the two eddies (Chen et al., 2016; He et al., 2016; Li et al., 2018). In both seasons, the surface waters in the study region were generally found to be nitrogen deficient, with NO_2^- at $< 0.01\text{--}0.04 \text{ } \mu\text{mol L}^{-1}$ (Figure S2a, S1b), NO_3^- at $< 0.03\text{--}2.82 \text{ } \mu\text{mol L}^{-1}$ (Figure S1a), and NH_4^+ at $0.04\text{--}0.35 \text{ } \mu\text{mol L}^{-1}$ (Figure S2b, S1c). The concentrations of NO_2^- and NO_3^- were below the detection limit at almost 80% of the sampling stations during both cruises. Due to the injection of shelf water with low salinity and abundant terrestrial nutrients, significant high concentrations of NO_3^- and NO_2^- were observed along Transect 3 in June 2015 (Figure S1a, S1b) where the shelf water was intruded by eddies (Chen et al., 2016; He et al., 2016). Such transport processes from the inner shelf to the slope region have a profound influence on nutrient dynamics and biological productions (He et al.,

删除的内容: water

2016). The water that was influenced by shelf water with a potential density anomaly lower than 20.25 kg m^{-3} and salinity lower than 33 had high concentrations of DIN (Figure 8a). At the 6 stations (in the red circle of Figure 8a) that were intruded by shelf water and characterized with surface salinity lower than 33, we obtained an average surface DIN concentration of $1.82 \pm 1.16 (0.27\text{--}3.01) \mu\text{mol L}^{-1}$, which was significantly higher than the mean of $0.10 \pm 0.03 (0.04\text{--}0.16) \mu\text{mol L}^{-1}$ at other stations (independent samples t-test, $p < 0.01$). After neglecting the two stations (J-14, J-15) influenced by upwelling, a strong correlation between NCP and DIN was observed in the cruise of June 2015 ($r = 0.747$, $p < 0.01$), with higher NCP (avg. $15.4 \pm 4.5 \text{ mmol C m}^{-2} \text{ d}^{-1}$) occurred at the stations where shelf water intruded, consistent with the DIN concentration higher than $0.27 \mu\text{mol L}^{-1}$ (Figure 8b). At other stations without the influence of shelf water, the average NCP was just $2.3 \pm 1.7 \text{ mmol C m}^{-2} \text{ d}^{-1}$. These results furtherly suggest that the supply of DIN from shelf water can greatly stimulate the primary production at these stations, resulting in the NCP increase of nearly 7 times compared to other stations.

The correlations between NCP and sea surface temperature and salinity also support the influence of physical forcing on NCP. In June 2015, we obtained a strong negative correlation between NCP and salinity (Figure 9d). NCP significantly increased in the water with salinity lower than 33 (Figure 9d). Temperature had weak correlations with NCP (Figure 9c), and the negative NCP values were concentrated in the water with temperatures below 30.5°C and salinity values over 33.5 (Figure 9c, 9d). This surface water was mostly observed along Transect 4 where vertical mixing caused by a cold eddy brought deep water to the surface. The undersaturated $\Delta(\text{O}_2/\text{Ar})$ entrained by deep water caused the negative NCP estimates at the surface, resulting in a considerable underestimation of NCP. Unlike in June 2015, all the correlations were very weak between NCP and temperature, salinity in October 2014 (Figure 9a, 9b). The Kuroshio water and the SCS water had similar hydrological characteristics and their mixing in October 2014 may not have resulted in significant changes in the hydrological characteristics of the surface water.

The nutrient concentrations and hydrographic characteristics we observed just reflect

删除的内容: s

the marine environment at the moment of sampling, partly contradicting our estimates that quantified NCP over a period prior to the observation. Especially for the regions with significant influence of shelf water in June 2015, tracking the history of shelf water intrusion is important. We used daily satellite chlorophyll data to monitor the intrusion of shelf water and roughly set satellite-chlorophyll $\geq \sim 0.2 \mu\text{g L}^{-1}$ as the criterion of shelf water (Figure 10). On 10 June 2015, shelf water began to influence the northern end (J-9) of Transect 3 and most part of Transect 4, then it extended to the southern end of Transect 3 and Transect 4 where J-12 and J-13 located on 13 June (Figure 1b, 10). Till 25 June when we finished the observation of Transect 4, the entire Transect 3 (J-9 to 12) as well as J-13 and J-16 had kept been dominated by shelf water for more than 10 days (Figure 1b, 10). We concluded these findings in Table 3, along with the residence time (τ) of O_2 in the mixed layer and the difference (Δday) between the date of observation and the start date of shelf water intrusion at the stations with surface salinity lower than 33. Δday can represent the duration of the shelf water intrusion at each station before our observation. The residence time of O_2 in the mixed layer at most stations listed in Table 3 is shorter than or equivalent to Δday . This result suggests that our estimate has appropriately integrated the NCP during the period of shelf water intrusion, which can effectively reflect the influence of shelf water on productive state on the northern slope of the SCS in the summer.

The amount of light may also play a role in the extent of primary production. The MLD is considered a driver of light availability in the mixed layer (Cassar et al., 2011; Hahm et al., 2014). The euphotic layer was averagely 40 m thicker than the mixed layer in the study region during the summer cruise, thus it's not very significant to discuss the light limitation in June 2015. We conducted an analysis of light availability based on daily satellite-PAR data and NCP in October 2014. To minimize the influence of DIN concentrations, we selected 9 stations where surface DIN concentration in the range of $0.10\text{--}0.17 \mu\text{mol L}^{-1}$. The average surface PAR ($\text{mol m}^{-2} \text{d}^{-1}$) at each station was integrated over the residence time of O_2 before our observation. Then an average PAR in the mixed layer was calculated based on K_d . At the selected stations, the surface PAR varies over a range of $38.6\text{--}42.2 \text{ mol m}^{-2} \text{d}^{-1}$, while the average PAR in the mixed

删除的内容: S3

删除的内容: the

删除的内容: S3

删除的内容: S3

删除的内容: Light may also play a role in the primary production.

layer (ML PAR) ranged from 8.7 to 13.3 mol m⁻² d⁻¹ (Table 4). There's no significant correlation between the average PAR and NCP in the mixed layer (Table 4), partly suggesting that light intensity may not be a factor on NCP in the autumn. Light availability in the northern slope region of SCS is enough to support the primary production of phytoplankton.

4 Conclusion

The distribution of $\Delta(\text{O}_2/\text{Ar})$ and NCP on the northern slope of the SCS was strongly affected by nutrient availability, especially nitrogen. The nitrogen limitation on NCP was found both in the autumn and summer. In June 2015, we observed strong biological responses to the supply of nitrogen induced by eddy-entrained shelf water intrusion. NCP in the region with the influence of shelf water was $23.8 \pm 10.7 \text{ mmol C m}^{-2} \text{ d}^{-1}$ on average, with a maximum of $61.4 \text{ mmol C m}^{-2} \text{ d}^{-1}$. In addition, vertical mixing caused considerable underestimation of NCP in the transect influenced by a cold eddy. Removing the regions with the influence of shelf water intrusion and vertical mixing, the average NCP in other regions was $5.0 \pm 6.2 \text{ mmol C m}^{-2} \text{ d}^{-1}$. This value agrees well with previously published NCP estimates for the study area. Our results also reveal the rapid response of ecosystem to physical processes. The summer shelf water intrusion may significantly promote NCP by potentially more than threefold in the study region. This is the first report that quantifies the contribution of shelf water intrusion to NCP on the northern slope of the SCS in the summer. Because of the sufficient illumination in the tropical SCS, light availability may not be a significant limitation on NCP in both seasons. The high-resolution NCP estimates derived from continuous measurement of O_2/Ar presented in this paper are of significance for understanding the carbon cycle in the highly dynamic system of the SCS.

Data Availability

All data presented in this manuscript are available on Weiyun.com (link: <https://share.weiyun.com/ZtbQMNGI>, password: p7rj36)

删除的内容: dynamic processes such as

删除的内容: the

删除的内容: errors

删除的内容: estimates

删除的内容: 376 %

删除的内容: s

Author contribution

Guiling Zhang and Yu Han designed and set up the underway measurement system. Wenjing Zheng attended both cruises (in June 2015 and October 2014) in the South China Sea, and was mainly responsible for operating the underway measurement system during the cruises. Sumei Liu provided the nutrients data of both cruises. Chuan Qin attended the cruise in June 2015 and prepared the manuscript with contributions from all co-authors.

Acknowledgments

The authors wish to thank the crew of the *R/V “Nanfeng”* for the assistance with the collection of field samples and Professor Xiaoxia Sun for providing the ^{14}C -PP data. We would also like to thank the Ocean Biology Processing Group (OBPG) of NASA for generating the PAR data and the E.U. Copernicus Marine Environment Monitoring Service (CMEMS) for providing the satellite chlorophyll data. Professor Michael Bender and Bror Jonsson are acknowledged for constructive suggestions on the continuous O_2/Ar measurement system and the calculation of O_2/Ar -based NCP. This study was funded by the National Science Foundation of China through Grant Nos. 41776122, by the Ministry of Science and Technology of China through Grant Nos. 2014CB441502, by the Fundamental Research Funds for the Central Universities (No. 201562010), and by the Taishan Scholars Programme of Shandong Province (No. 201511014) and the Aoshan Talents Programme of the Qingdao National Laboratory for Marine Science and Technology (No. 2015ASTP-OS08).

Competing interests

The authors declare that they have no conflict of interest.

References:

- Bi, Q., Du, J., Wu, Y., Zhou, J. and Zhang, J.: Particulate organic carbon export flux by $^{234}\text{Th}/^{238}\text{U}$ disequilibrium in the continental slope of the East China Sea, *Acta Oceanol. Sin.*, 32(10), 67–73, doi:10.1007/s13131-013-0303-7, 2013.
- Cai, P., Zhao, D., Wang, L., Huang, B. and Dai, M.: Role of particle stock and phytoplankton community structure in regulating particulate organic carbon export in a large marginal sea, *J. Geophys. Res. Oceans*, 120(3), 2063–2095, doi:10.1002/2014JC010432, 2015.
- Cai, W.: Estuarine and Coastal Ocean Carbon Paradox: CO_2 Sinks or Sites of Terrestrial Carbon Incineration?, *Ann. Rev. Mar. Sci.*, 3(1), 123–145, doi:10.1146/annurev-marine-120709-142723, 2011.
- Cassar, N., Difiore, P. J., Barnett, B. A., Bender, M. L., Bowie, A. R., Tilbrook, B., Petrou, K., Westwood, K. J., Wright, S. W. and Lefevre, D.: The influence of iron and light on net community production in the Subantarctic and Polar Frontal Zones, *Biogeosciences*, 8(2), 227–237, doi:10.5194/bg-8-227-2011, 2011.
- Cassar, N., Nevison, C. D. and Manizza, M.: Correcting oceanic O_2/Ar -net community production estimates for vertical mixing using N_2O observations, *Geophys. Res. Lett.*, 41(24), 8961–8970, doi:10.1002/2014GL062040, 2014.
- Chen, J., Zheng, L., Wiesner, M. G., Chen, R., Zheng, Y. and Wong, H.: Estimations of primary production and export production in the South China Sea based on sediment trap experiments, *Chinese Sci. Bull.*, 43(7), 583–586, doi:10.1007/BF02883645, 1998.
- Chen, W., Cai, P., Dai, M. and Wei, J.: $^{234}\text{Th}/^{238}\text{U}$ disequilibrium and particulate organic carbon export in the northern South China Sea, *J. Oceanogr.*, 64(3), 417–428, doi:10.1007/s10872-008-0035-z, 2008.
- Chen, Y. and Tang, D.: Eddy-feature phytoplankton bloom induced by a tropical cyclone in the South China Sea, *Int. J. Remote Sens.*, 33(23), 7444–7457, doi:10.1080/01431161.2012.685976, 2012.
- Chen, Z., Yang, C., Xu, D. and Xu, M.: Observed hydrographical features and circulation with influences of cyclonic-anticyclonic eddy-pair in the northern slope of the South China Sea during June 2015 (in Chinese), *J. Mar. Sci.*, 34(4), 10–19, doi:10.3969/j.issn.1001-909X.2016.04.002, 2016.

2016.

Cheng, G., Sun, J., Zu, T., Chen, J. and Wang, D.: Analysis of water masses in the northern South China Sea in summer 2011 (in Chinese), *J. Trop. Oceanogr.*, 33(3), 10–16, doi:10.3969/j.issn.1009-5470.2014.03.002, 2014.

Chou, W., Lee Chen, Y., Sheu, D., Shih, Y., Han, C., Cho, C., Tseng, C. and Yang, Y.: Estimated net community production during the summertime at the SEATS time-series study site, northern South China Sea: Implications for nitrogen fixation, *Geophys. Res. Lett.*, 33(22), doi:10.1029/2005GL025365, 2006.

Clark, D. R., Rees, A. P. and Joint, I.: Ammonium regeneration and nitrification rates in the oligotrophic Atlantic Ocean: Implications for new production estimates, *Limnol. Oceanogr.*, 53(1), 52–62, doi:10.4319/lo.2008.53.1.0052, 2008.

Craig, H. and Hayward, T.: Oxygen Supersaturation in the Ocean: Biological Versus Physical Contributions, *Science*, 235(4785), 199–202, doi:10.1126/science.235.4785.199, 1987.

Dugdale, R. C. and Goering, J. J.: Uptake of New and Regenerated Forms of Nitrogen in Primary Productivity, *Limnol. Oceanogr.*, 12(2), 196–206, doi:10.4319/lo.1967.12.2.0196, 1967.

[Emerson, S., Quay, P., Stump, C., Wilbur, D. and Knox, M.: O₂, Ar, N₂, and ²²²Rn in surface waters of the subarctic Ocean: Net biological O₂ production, *Global Biogeochem. Cycles*, 5\(1\), 49–69, doi:10.1029/90GB02656, 1991.](#)

Eveleth, R., Cassar, N., Sherrell, R. M., Ducklow, H., Meredith, M. P., Venables, H. J., Lin, Y. and Li, Z.: Ice melt influence on summertime net community production along the Western Antarctic Peninsula, *Deep Sea Res. Part II Top. Stud. Oceanogr.*, 139, 89–102, doi:10.1016/j.dsr2.2016.07.016, 2017.

Fan, L., Su, Y. and Li, F.: Analysis on water masses in the Northern South China Sea (in Chinese), *Acta Oceanol. Sin.*, 10(2), 136–145, 1988.

Feng, S., Li, F. and Li, S.: An introduction to marine science (in Chinese), Higher Education Press, Beijing, China., 1999.

Giesbrecht, K. E., Hamme, R. C. and Emerson, S. R.: Biological productivity along Line P in the subarctic northeast Pacific: In situ versus incubation-based methods, *Global Biogeochem. Cycles*, 26(3), doi:10.1029/2012GB004349, 2012.

Grande, K. D., Williams, P. J. L. B., Marra, J., Purdie, D. A., Heinemann, K., Eppley, R. W. and

Bender, M. L.: Primary production in the North Pacific gyre: a comparison of rates determined by the ^{14}C , O_2 concentration and ^{18}O methods, *Deep Sea Res. Part A, Oceanogr. Res. Pap.*, 36(11), 1621–1634, doi:10.1016/0198-0149(89)90063-0, 1989.

Guéguen, C. and Tortell, P. D.: High-resolution measurement of Southern Ocean CO_2 and O_2/Ar by membrane inlet mass spectrometry, *Mar. Chem.*, 108(3–4), 184–194, doi:10.1016/j.marchem.2007.11.007, 2008.

Hahm, D., Rhee, T. S., Kim, H. C., Park, J., Kim, Y. N., Shin, H. C. and Lee, S.: Spatial and temporal variation of net community production and its regulating factors in the Amundsen Sea, Antarctica, *J. Geophys. Res. Oceans*, 119(5), 2815–2826, doi:10.1002/2013JC009762, 2014.

Hamme, R. C., Cassar, N., Lance, V. P., Vaillancourt, R. D., Bender, M. L., Strutton, P. G., Moore, T. S., DeGrandpre, M. D., Sabine, C. L., Ho, D. T. and Hargreaves, B. R.: Dissolved O_2/Ar and other methods reveal rapid changes in productivity during a Lagrangian experiment in the Southern Ocean, *J. Geophys. Res. Oceans*, 117(C4), 92–99, doi:10.1029/2011JC007046, 2012.

Han, A., Dai, M., Gan, J., Kao, S., Zhao, X., Jan, S., Li, Q., Lin, H., Chen, C., Wang, L., Hu, J., Wang, L. and Gong, F.: Inter-shelf nutrient transport from the East China Sea as a major nutrient source supporting winter primary production on the northeast South China Sea shelf, *Biogeosciences*, 10(12), 8159–8170, doi:10.5194/bg-10-8159-2013, 2013.

Hanson, C. E., Pesant, S., Waite, A. M. and Pattiaratchi, C. B.: Assessing the magnitude and significance of deep chlorophyll maxima of the coastal eastern Indian Ocean, *Deep. Res. Part II Top. Stud. Oceanogr.*, 54(8–10), 884–901, doi:10.1016/j.dsr2.2006.08.021, 2007.

He, X., Xu, D., Bai, Y., Pan, D., Chen, C. A., Chen, X. and Gong, F.: Eddy-entrained Pearl River plume into the oligotrophic basin of the South China Sea, *Cont. Shelf Res.*, 124, 117–124, doi:10.1016/j.csr.2016.06.003, 2016.

[Hendricks, M. B., Bender, M. L. and Barnett, B. A.: Net and gross \$\text{O}_2\$ production in the southern ocean from measurements of biological \$\text{O}_2\$ saturation and its triple isotope composition, *Deep. Res. Part I Oceanogr. Res. Pap.*, 51\(11\), 1541–1561, doi:10.1016/j.dsr.2004.06.006, 2004.](#)

Hu, J., Kawamura, H., Hong, H. and Qi, Y.: A Review on the currents in the South China Sea: Seasonal circulation, South China Sea warm current and Kuroshio intrusion, *J. Oceanogr.*, 56(6), 607–624, doi:10.1023/A:1011117531252, 2000.

[Huang, K., Ducklow, H., Vernet, M., Cassar, N. and Bender, M. L.: Export production and its](#)

739 [regulating factors in the West Antarctica Peninsula region of the Southern Ocean, Global](#)
740 [Biogeochem. Cycles, 26\(2\), doi:10.1029/2010GB004028, 2012.](#)

741 Huang, Y., Yang, B., Chen, B., Qiu, G., Wang, H. and Huang, B.: Net community production in the
742 South China Sea Basin estimated from in situ O₂ measurements on an Argo profiling float, Deep
743 Sea Res. Part I Oceanogr. Res. Pap., 131, 54–61, doi:10.1016/j.dsr.2017.11.002, 2018.

744 Izett, R. W., Manning, C. C., Hamme, R. C. and Tortell, P. D.: Refined Estimates of Net Community
745 Production in the Subarctic Northeast Pacific Derived From $\Delta\text{O}_2/\text{Ar}$ Measurements With N₂O-
746 Based Corrections for Vertical Mixing, Global Biogeochem. Cycles, 32(3), 326–350,
747 doi:10.1002/2017GB005792, 2018.

748 Jiang, Z., Huang, C., Dai, M., Kao, S., Hydes, D. J., Chou, W. and Janf, S.: Short-term dynamics of
749 oxygen and carbon in productive nearshore shallow seawater systems off Taiwan: Observations and
750 modeling, Limnol. Oceanogr., 56(5), 1832–1849, doi:10.4319/lo.2011.56.5.1832, 2011.

751 Jonsson, B. F., Doney, S. C., Dunne, J. and Bender, M.: Evaluation of the Southern Ocean O₂/Ar-
752 based NCP estimates in a model framework, J. Geophys. Res. Biogeosciences, 118(2), 385–399,
753 doi:10.1002/jgrg.20032, 2013.

754 Jerlov, N. G.: Marine optics, Elsevier, Netherlands, 1976.

755 Kaiser, J., Reuer, M. K., Barnett, B. and Bender, M. L.: Marine productivity estimates from
756 continuous O₂/Ar ratio measurements by membrane inlet mass spectrometry, Geophys. Res. Lett.,
757 32(19), 1–5, doi:10.1029/2005GL023459, 2005.

758 Kirk, J. T.: Light and photosynthesis in aquatic ecosystems, Cambridge university press, UK, 1994.

759 La Roche, J.: Ammonium regeneration: its contribution to phytoplankton nitrogen requirements in
760 a eutrophic environment, Mar. Biol., 75(2–3), 231–240, doi:10.1007/BF00406007, 1983.

761 Lee Chen, Y.: Spatial and seasonal variations of nitrate-based new production and primary
762 production in the South China Sea, Deep Sea Res. Part I Oceanogr. Res. Pap., 52(2), 319–340,
763 doi:10.1016/j.dsr.2004.11.001, 2005.

764 Lee Chen, Y. and Chen, H.: Seasonal dynamics of primary and new production in the northern South
765 China Sea: The significance of river discharge and nutrient advection, Deep Sea Res. Part I
766 Oceanogr. Res. Pap., 53(6), 971–986, doi:10.1016/j.dsr.2006.02.005, 2006.

767 Li, D., Zhou, M., Zhang, Z., Zhong, Y., Zhu, Y., Yang, C., Xu, M., Xu, D. and Hu, Z.: Intrusions
768 of Kuroshio and Shelf Waters on Northern Slope of South China Sea in Summer 2015, J. Ocean

Univ. China, 17(3), 477–486, doi:10.1007/s11802-018-3384-2, 2018.

Li, Q., Guo, X., Zhai, W., Xu, Y. and Dai, M.: Partial pressure of CO₂ and air-sea CO₂ fluxes in the South China Sea: Synthesis of an 18-year dataset, *Prog. Oceanogr.*, 182, doi:10.1016/j.pocean.2020.102272, 2020.

Liao, X., Dai, M., Gong, X., Liu, X. and Huang, H.: Subsurface chlorophyll a maximum and its possible causes in the southern South China Sea, *J. Trop. Oceanogr.*, 37(1), 45–56, doi:10.11978/2017020, 2018.

Lin, X., Guan, Y. and Liu, Y.: Three-dimensional structure and evolution process of Dongsha Cold Eddy during autumn 2000 (in Chinese), *J. Trop. Oceanogr.*, 32(2), 55–65, doi:10.3969/j.issn.1009-5470.2013.02.006, 2013.

Liu, M., Liu, X., Ma, A., Li, T. and Du, Z.: Spatio-temporal stability and abnormality of chlorophyll-a in the northern south china sea during 2002–2012 from MODIS images using wavelet analysis, *Cont. Shelf Res.*, 75, 15–27, doi:10.1016/j.csr.2013.12.010, 2014.

Lockwood, D., Quay, P. D., Kavanaugh, M. T., Juranek, L. W. and Feely, R. A.: High-resolution estimates of net community production and air-sea CO₂ flux in the northeast Pacific, *Global Biogeochem. Cycles*, 26(4), doi:10.1029/2012GB004380, 2012.

Ma, H., Zeng, Z., He, J., Chen, L., Yin, M., Zeng, S. and Zeng, W.: Vertical flux of particulate organic carbon in the central South China Sea estimated from ²³⁴Th-²³⁸U disequilibria, *Chinese J. Oceanol. Limnol.*, 26(4), 480–485, doi:10.1007/s00343-008-0480-y, 2008.

Ma, H., Zeng, Z., Yu, W., He, J., Chen, L., Cheng, J., Yin, M. and Zeng, S.: ²³⁴Th/ ²³⁸U disequilibrium and particulate organic carbon export in the northwestern South China Sea, *Acta Oceanol. Sin.*, 30(3), 55–62, doi:10.1007/s13131-011-0119-2, 2011.

Manning, C. C., Stanley, R. H. R., Nicholson, D. P., Smith, J. M., Timothy Pennington, J., Fewings, M. R., Squibb, M. E. and Chavez, F. P.: Impact of recently upwelled water on productivity investigated using in situ and incubation-based methods in Monterey Bay, *J. Geophys. Res. Oceans*, 122(3), 1901–1926, doi:10.1002/2016JC012306, 2017.

Mathis, J. T., Cross, J. N. and Bates, N. R.: Coupling primary production and terrestrial runoff to ocean acidification and carbonate mineral suppression in the eastern Bering Sea, *J. Geophys. Res. Ocean.*, 116(2), doi:10.1029/2010JC006453, 2011.

Millero, F. J. and Poisson, A.: International one-atmosphere equation of state of seawater, *Deep Sea*

799 Res. Part A, Oceanogr. Res. Pap., 28(6), 625–629, doi:10.1016/0198-0149(81)90122-9, 1981.

800 Monterey, G. and Levitus, S.: Seasonal Variability of Mixed Layer Depth, NOAA Atlas NEDIS 14,
801 U.S. Gov. Printing Off. D.C. [online] Available from: <http://www.nodc.noaa.gov>, 1997.

802 [NASA Goddard Space Flight Center, Ocean Ecology Laboratory, Ocean Biology Processing Group:](#)
803 [Moderate-resolution Imaging Spectroradiometer \(MODIS\) Aqua Photosynthetically Available](#)
804 [Radiation Data, NASA OB DAAC, Greenbelt, MD, USA. doi:](#)
805 [data/10.5067/AQUA/MODIS/L3M/PAR/2018_2018 Reprocessing.](#)

806 Nemcek, N., Ianson, D. and Tortell, P. D.: A high-resolution survey of DMS, CO₂, and O₂/Ar
807 distributions in productive coastal waters, Global Biogeochem. Cycles, 22(2),
808 doi:10.1029/2006GB002879, 2008.

809 Ning, X., Chai, F., Xue, H., Cai, Y., Liu, C. and Shi, J.: Physical-biological oceanographic coupling
810 influencing phytoplankton and primary production in the South China Sea, J. Geophys. Res. Oceans,
811 109(10), doi:10.1029/2004JC002365, 2004.

812 Ning, X., Peng, X., Le, F., Hao, Q., Sun, J., Liu, C. and Cai, Y.: Nutrient limitation of phytoplankton
813 in anticyclonic eddies of the northern South China Sea, Biogeosciences Discuss., 5(6), 4591–4619,
814 doi:10.5194/bgd-5-4591-2008, 2008.

815 Pan, X., Wong, G. T. F., Shiah, F. K. and Ho, T. Y.: Enhancement of biological productivity by
816 internal waves: Observations in the summertime in the northern South China Sea, J. Oceanogr.,
817 68(3), 427–437, doi:10.1007/s10872-012-0107-y, 2012.

818 Parsons, T. R., Maita, Y. and Lalli, C. M.: A Manual of Chemical & Biological Methods for
819 Seawater Analysis, Pergamon Press, Oxford, UK., 1984.

820 [Pawlowicz, R.: M_Map: A mapping package for MATLAB, version 1.4m, \[online\] Available from:](#)
821 [www.eoas.ubc.ca/~rich/map.html, 2020.](#)

822 Quay, P. D., Peacock, C., Bjrkman, K. and Karl, D. M.: Measuring primary production rates in the
823 ocean: Enigmatic results between incubation and non-incubation methods at Station ALOHA,
824 Global Biogeochem. Cycles, 24(3), doi:10.1029/2009GB003665, 2010.

825 Rehder, G. and Suess, E.: Methane and pCO₂ in the Kuroshio and the South China Sea during
826 maximum summer surface temperatures, Mar. Chem., 75(1–2), 89–108, doi:10.1016/S0304-
827 4203(01)00026-3, 2001.

828 Reuer, M. K., Barnett, B. A., Bender, M. L., Falkowski, P. G. and Hendricks, M. B.: New estimates

删除的内容: .

830 of Southern Ocean biological production rates from O₂/Ar ratios and the triple isotope composition
831 of O₂, Deep Sea Res. Part I Oceanogr. Res. Pap., 54(6), 951–974, doi:10.1016/j.dsr.2007.02.007,
832 2007.

833 Shadwick, E. H., Tilbrook, B., Cassar, N., Trull, T. W. and Rintoul, S. R.: Summertime physical
834 and biological controls on O₂ and CO₂ in the Australian Sector of the Southern Ocean, J. Mar. Syst.,
835 147, 21–28, doi:10.1016/j.jmarsys.2013.12.008, 2015.

836 Shi, X., Li, H., Han, X., Wang, L. and Zhu, C.: Influence of typical mesoscale oceanographical
837 process on the distribution of nutrients and dissolved oxygen in the Northern part of South China
838 Sea in summer (in Chinese), Acta Sci. Circumstantiae, 34(3), 695–703,
839 doi:10.13671/j.hjkxxb.2014.0121, 2014.

840 Stanley, R. H. R., Kirkpatrick, J. B., Cassar, N., Barnett, B. A. and Bender, M. L.: Net community
841 production and gross primary production rates in the western equatorial Pacific, Global Biogeochem.
842 Cycles, 24(4), doi:10.1029/2009GB003651, 2010.

843 Su, J. and Yuan, Y.: Coastal hydrology of China (in Chinese), China Ocean Press, Beijing, China.,
844 2005.

845 Takahashi, T., Sutherland, S. C., Wanninkhof, R., Sweeney, C., Feely, R. A., Chipman, D. W.,
846 Hales, B., Friederich, G., Chavez, F., Sabine, C., Watson, A., Bakker, D. C. E., Schuster, U., Metzl,
847 N., Yoshikawa-Inoue, H., Ishii, M., Midorikawa, T., Nojiri, Y., Körtzinger, A., Steinhoff, T.,
848 Hoppema, M., Olafsson, J., Arnarson, T. S., Tilbrook, B., Johannessen, T., Olsen, A., Bellerby, R.,
849 Wong, C. S., Delille, B., Bates, N. R. and de Baar, H. J. W.: Climatological mean and decadal
850 change in surface ocean pCO₂, and net sea–air CO₂ flux over the global oceans, Deep Sea Res. Part
851 II Top. Stud. Oceanogr., 56(8–10), 554–577, doi:10.1016/j.dsr.2008.12.009, 2009.

852 Tamminen, T.: Effects of ammonium effluents on planktonic primary production and
853 decomposition in a coastal brackish water environment I. Nutrient balance of the water body and
854 effluent tests, Netherlands J. Sea Res., 16(C), 455–464, doi:10.1016/0077-7579(82)90050-3, 1982.

855 Teeter, L., Hamme, R. C., Ianson, D. and Bianucci, L.: Accurate Estimation of Net Community
856 Production From O₂/Ar Measurements, Global Biogeochem. Cycles, 32(8), 1163–1181,
857 doi:10.1029/2017GB005874, 2018.

858 Teira, E., Mouriño, B., Maraño, E., Pérez, V., Pazó, M. J., Serret, P., De Armas, D., Escánez, J.,
859 Woodward, E. M. S. and Fernández, E.: Variability of chlorophyll and primary production in the

860 Eastern North Atlantic Subtropical Gyre: Potential factors affecting phytoplankton activity, *Deep.*
861 *Res. Part I Oceanogr. Res. Pap.*, 52(4), 569–588, doi:10.1016/j.dsr.2004.11.007, 2005.

862 Tortell, P. D.: Dissolved gas measurements in oceanic waters made by membrane inlet mass
863 spectrometry, *Limnol. Oceanogr. Methods*, 3(1), 24–37, doi:10.4319/lom.2005.3.24, 2005.

864 Tortell, P. D., Asher, E. C., Ducklow, H. W., Goldman, J. A. L., Dacey, J. W. H., Grzyski, J. J.,
865 Young, J. N., Kranz, S. A., Bernard, K. S. and Morel, F. M. M.: Metabolic balance of coastal
866 Antarctic waters revealed by autonomous $p\text{CO}_2$ and $\Delta\text{O}_2/\text{Ar}$ measurements, *Geophys. Res. Lett.*,
867 41(19), 6803–6810, doi:10.1002/2014GL061266, 2014.

868 Tortell, P. D., Merzouk, A., Ianson, D., Pawlowicz, R. and Yelland, D. R.: Influence of regional
869 climate forcing on surface water $p\text{CO}_2$, $\Delta\text{O}_2/\text{Ar}$ and dimethylsulfide (DMS) along the southern
870 British Columbia coast, *Cont. Shelf Res.*, 47, 119–132, doi:10.1016/j.csr.2012.07.007, 2012.

871 Ulfso, A., Cassar, N., Korhonen, M., Van Heuven, S., Hoppema, M., Kattner, G. and Anderson, L.
872 G.: Late summer net community production in the central Arctic Ocean using multiple approaches,
873 *Global Biogeochem. Cycles*, 28(10), 1129–1148, doi:10.1002/2014GB004833, 2014.

874 Uu, D. V. and Brankart, J. M.: Seasonal variation of temperature and salinity fields and water masses
875 in the Bien Dong (South China) Sea, *Math. Comput. Model.*, 26(12), 97–113, doi:10.1016/S0895-
876 7177(97)00243-4, 1997.

877 Wang, N., Lin, W., Cheng, B. and Huang, B.: Metabolic states of the Taiwan Strait and the northern
878 South China Sea in summer 2012 (in Chinese), *J. Trop. Oceanogr.*, 33(4), 61–68,
879 doi:10.3969/j.issn.1009-5470.2014.04.008, 2014.

880 Wanninkhof, R.: Relationship between wind speed and gas exchange over the ocean, *J. Geophys.*
881 *Res. Oceans*, 97(C5), 7373–7382, doi:10.1029/92JC00188, 1992.

882 Weiss, R. F.: The solubility of nitrogen, oxygen and argon in water and seawater, *Deep Sea Res.*
883 *Oceanogr. Abstr.*, 17(4), 721–735, doi:10.1016/0011-7471(70)90037-9, 1970.

884 Zhai, W., Dai, M. and Cai, W.: Coupling of surface $p\text{CO}_2$ and dissolved oxygen in the northern
885 South China Sea: Impacts of contrasting coastal processes, *Biogeosciences*, 6(11), 2589–2598,
886 doi:10.5194/bg-6-2589-2009, 2009.

887 Zhang, R., Zhu, X., Yang, C., Ye, L., Zhang, G., Ren, J., Wu, Y., Liu, S., Zhang, J. and Zhou, M.:
888 Distribution of dissolved iron in the Pearl River (Zhujiang) Estuary and the northern continental
889 slope of the South China Sea, *Deep. Res. Part II Top. Stud. Oceanogr.*, 167, 14–24,

890 doi:10.1016/j.dsr2.2018.12.006, 2019.

891

892

893 **Table Captions:**

894 **Table 1.** Basic information at all CTD stations in October 2014

895 **Table 2.** Basic information at all CTD stations in June 2015

896 **Table 3.** The start date and duration (Δ day) of shelf water intrusion at [the](#) stations with surface
897 salinity lower than 33 in June 2015

898 **Table4.** Satellite-PAR data and NCP at the selected stations in October 2014

899

Figure Captions:

Figure 1. Cruise tracks of two cruises in the slope region of the Northern South China Sea in (a) October 2014, (b) June 2015. The sea level height anomaly (SLA) and geostrophic current during observations in June 2015 (Chen et al., 2016) are shown in (c). The black dots/stars represent the locations of the CTD casts. Red numbers indicate transects, while black numbers indicate the serial number of CTD stations based on the cruise plan. The color scale in (a) and (b) represents bathymetry.

Figure 2. Surface distributions of (a) temperature, (b) salinity, (c) chlorophyll-a (Chl a), and (d) $\Delta(\text{O}_2/\text{Ar})$ in October 2014

Figure 3. Surface distributions of (a) temperature, (b) salinity, (c) chlorophyll-a (Chl a), (d) dissolved oxygen (DO), (e) $p\text{CO}_2$, and (f) $\Delta(\text{O}_2/\text{Ar})$ in June 2015

Figure 4. Surface distribution of NCP among the northern slope of SCS during the cruise in (a) October 2014 and (b) June 2015.

Figure 5. Zonal variations in (a) temperature, salinity, (b) $\Delta(\text{O}_2/\text{Ar})$, (c) Chl a, NCP and surface concentration of ammonia (NH_4^+) along Transect 5 in October 2014. The plots of $\Delta(\text{O}_2/\text{Ar})$ and NCP are 10-point Savitzky-Golay smoothed to give a better view of their distribution.

Figure 6. Meridional variations in (a) temperature, salinity, (b) $\Delta(\text{O}_2/\text{Ar})$, $p\text{CO}_2$, (c) Chl a, NCP and surface concentration of DIN along Transect 4 in June 2015. The plots of $\Delta(\text{O}_2/\text{Ar})$, $p\text{CO}_2$ and NCP are 10-point Savitzky-Golay smoothed.

Figure 7. Principal Component Analysis (PCA) among variables for (a) October 2014 and (b) June 2015 (Bartlett's test of sphericity: $p < 0.01$)

Figure 8. (a) T-S diagram of surface DIN concentration in June 2015. The stations influenced by shelf water were in the red circle. **(b)** Correlation analysis between surface DIN concentration and NCP at sampling stations. The stations (characterized with $S < 33$) influenced by shelf water presented surface DIN concentration $\geq 0.27 \mu\text{mol L}^{-1}$.

Figure 9. Correlation analysis between underway NCP and physical parameters (temperature and salinity) in October 2014 (a, b) and June 2015 (c, d).

Figure 10. Daily satellite-chlorophyll images on the selected days in June 2015. Stars represent CTD locations. We roughly set satellite-chlorophyll $\geq 0.2 \mu\text{g L}^{-1}$ in this figure as the criterion of

929 [shelf water. This figure was made based on the M_Map mapping package for MATLAB \(Pawlowicz,](#)
930 [2020\).](#)

Table 1. Basic information at all CTD stations in October 2014

Station	Date of observation ^a	MLD (m)	Z _{eu} ^b (m)	k ^c (m d ⁻¹)	τ ^d (d)
O-01	13 Oct 2014	58	82	4.7	12
O-02	13 Oct 2014	64	74	5.2	12
O-03	14 Oct 2014	56	84	6.2	9
O-04	14 Oct 2014	54	76	6.3	9
O-05	20 Oct 2014	27	70	7.9	3
O-06	19 Oct 2014	55	62	8.4	7
O-07	21 Oct 2014	40	60	7.3	5
O-08	21 Oct 2014	49	72	7.4	7
O-09	15 Oct 2014	79	96	6.2	13
O-10	15 Oct 2014	68	81	6.1	11
O-11	15 Oct 2014	64	81	5.4	12
O-12	16 Oct 2014	66	74	5.2	13
O-13	16 Oct 2014	48	52	6.3	8
O-14	17 Oct 2014	54	62	6.9	8
O-15	22 Oct 2014	49	68	7.0	7
O-16	22 Oct 2014	50	73	7.3	7
O-17	23 Oct 2014	52	75	7.9	7
O-19	18 Oct 2014	31	64	9.4	3
O-20	18 Oct 2014	35	61	8.7	4
O-21	18 Oct 2014	81	86	6.9	12
O-22	17 Oct 2014	76	102	6.0	13

^a All dates are in the format of day, month, year. ^b Euphotic depth, defined based on subsurface chlorophyll maximum layer. ^c Gas transfer velocity of O₂. ^d Residence time of O₂ in the mixed layer, estimated as per MLD/k.

删除的内容: 2014/10/13

删除的内容: 2014/10/13

删除的内容: 2014/10/14

删除的内容: 2014/10/14

删除的内容: 2014/10/20

删除的内容: 2014/10/19

删除的内容: 2014/10/21

删除的内容: 2014/10/21

删除的内容: 2014/10/15

删除的内容: 2014/10/15

删除的内容: 2014/10/15

删除的内容: 2014/10/16

删除的内容: 2014/10/16

删除的内容: 2014/10/17

删除的内容: 2014/10/22

删除的内容: 2014/10/22

删除的内容: 2014/10/23

删除的内容: 2014/10/18

删除的内容: 2014/10/18

删除的内容: 2014/10/18

删除的内容: 2014/10/17

删除的内容: year...ay/...month/...day

...

978

Table 2. Basic information at all CTD stations in June 2015

Station	Date of observation	MLD (m)	Z_{eu} (m)	k (m d ⁻¹)	τ (d)
J-01	18 Jun 2015	26	63	2.2	12
J-02	17 Jun 2015	19	80	1.9	10
J-03	16 Jun 2015	20	74	1.9	11
J-04	15 Jun 2015	22	74	1.9	11
J-05	15 Jun 2015	11	78	1.2	9
J-06	14 Jun 2015	24	76	2.1	11
J-07	13 Jun 2015	21	81	2.3	9
J-08	18 Jun 2015	14	56	1.7	8
J-09	19 Jun 2015	17	59	1.6	10
J-10	19 Jun 2015	8	46	1.4	6
J-11	20 Jun 2015	8	40	2.8	3
J-12	21 Jun 2015	16	45	3.0	5
J-13	21 Jun 2015	19	45	2.3	8
J-14	24 Jun 2015	28	55	4.0	7
J-15	24 Jun 2015	17	42	5.3	3
J-16	25 Jun 2015	10	19	5.7	2

删除的内容: 2015/6/18

删除的内容: 2015/6/17

删除的内容: 2015/6/16

删除的内容: 2015/6/15

删除的内容: 2015/6/15

删除的内容: 2015/6/14

删除的内容: 2015/6/13

删除的内容: 2015/6/18

删除的内容: 2015/6/19

删除的内容: 2015/6/19

删除的内容: 2015/6/20

删除的内容: 2015/6/21

删除的内容: 2015/6/21

删除的内容: 2015/6/24

删除的内容: 2015/6/24

删除的内容: 2015/6/25

979

980

997
998
999

Table 3. The start date and duration (Δ day) of shelf water intrusion at the stations with surface salinity lower than 33 in June 2015

Station	Date of observation	Start date of shelf water intrusion	Δ day ^a	τ (d)
J-09	19 Jun 2015	10 Jun 2015	9	10
J-10	19 Jun 2015	13 Jun 2015	6	6
J-11	20 Jun 2015	13 Jun 2015	7	3
J-12	21 Jun 2015	13 Jun 2015	8	5
J-13	21 Jun 2015	13 Jun 2015	8	8
J-16	25 Jun 2015	before 10 Jun 2015	> 15	2

^a The difference between the date of observation and the start date of shelf water intrusion at listed stations.

删除的内容: at

带格式表格

删除的内容: 2015/6/19

删除的内容: 2015/6/10

删除的内容: 2015/6/19

删除的内容: 2015/6/13

删除的内容: 2015/6/20

删除的内容: 2015/6/13

删除的内容: 2015/6/21

删除的内容: 2015/6/13

删除的内容: 2015/6/21

删除的内容: 2015/6/13

删除的内容: 2015/6/25

删除的内容: 2015/6/10

Table 4. Satellite-PAR data and NCP at the selected stations in October 2014

Station	Date of observation	MLD (m)	Z _{eu} (m)	Surface PAR ^a (mol m ⁻² d ⁻¹)	K _d (m ⁻¹)	ML PAR ^b (mol m ⁻² d ⁻¹)	NCP (mmol C m ⁻² d ⁻¹)
O-01	13 Oct 2014	58	82	42.0	5.6 * 10 ⁻²	12.0	3.0
O-02	13 Oct 2014	64	74	42.0	6.2 * 10 ⁻²	10.0	15.1
O-03	14 Oct 2014	56	84	41.1	5.5 * 10 ⁻²	12.4	10.1
O-08	21 Oct 2014	49	72	38.7	6.4 * 10 ⁻²	11.4	15.7
O-10	15 Oct 2014	68	81	40.0	5.7 * 10 ⁻²	9.8	4.4
O-13	16 Oct 2014	48	52	39.2	8.9 * 10 ⁻²	8.7	15.3
O-15	22 Oct 2014	49	68	38.6	6.8 * 10 ⁻²	10.8	16.3
O-20	18 Oct 2014	35	61	39.2	7.5 * 10 ⁻²	13.3	16.4
O-22	17 Oct 2014	76	102	42.2	4.5 * 10 ⁻²	11.6	15.7

^a Average surface PAR over the residence time of O₂ in the mixed layer. ^b Average PAR in the mixed layer.

删除的内容: 2014/10/13

删除的内容: 2014/10/13

删除的内容: 2014/10/14

删除的内容: 2014/10/21

删除的内容: 2014/10/15

删除的内容: 2014/10/16

删除的内容: 2014/10/22

删除的内容: 2014/10/18

删除的内容: 2014/10/17

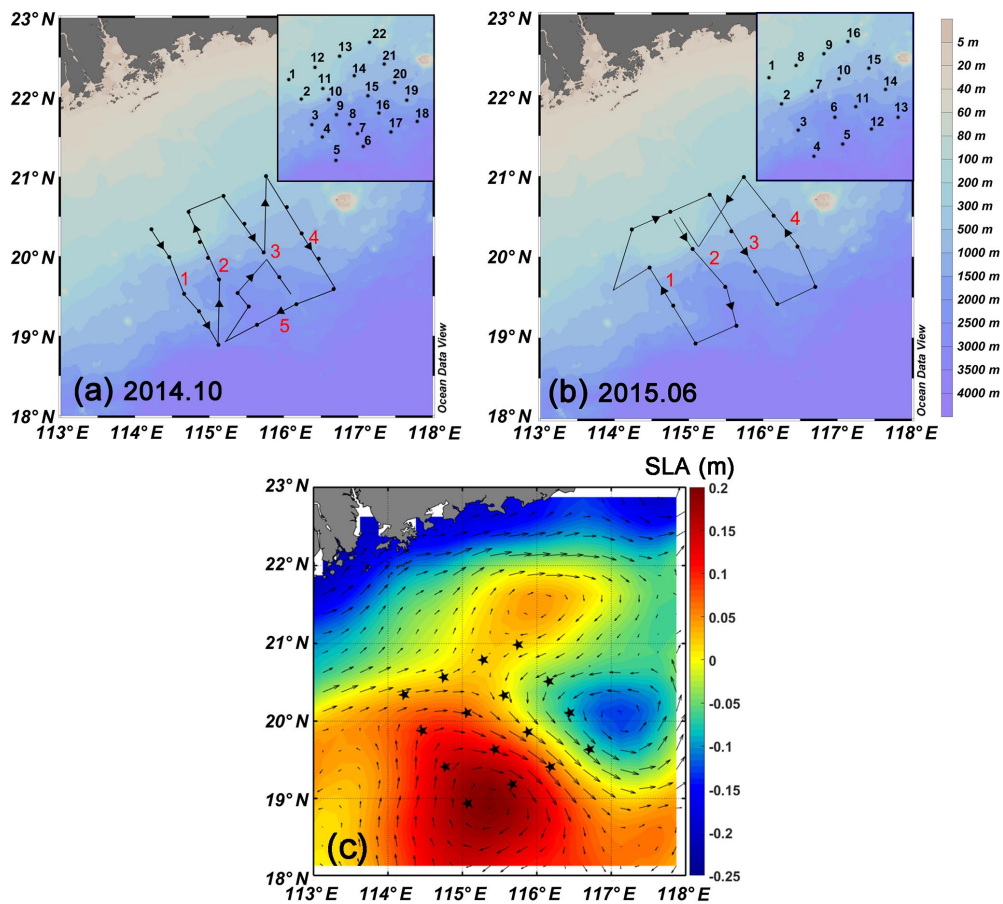


Figure 1. Cruise tracks of two cruises in the slope region of the Northern South China Sea in **(a)** October 2014, **(b)** June 2015. The sea level height anomaly (SLA) and geostrophic current during observations in June 2015 (Chen et al., 2016) are shown in **(c)**. The black dots/stars represent the locations of the CTD casts. Red numbers indicate transects, while black numbers indicate the serial number of CTD stations based on the cruise plan. The color scale in **(a)** and **(b)** represents bathymetry.

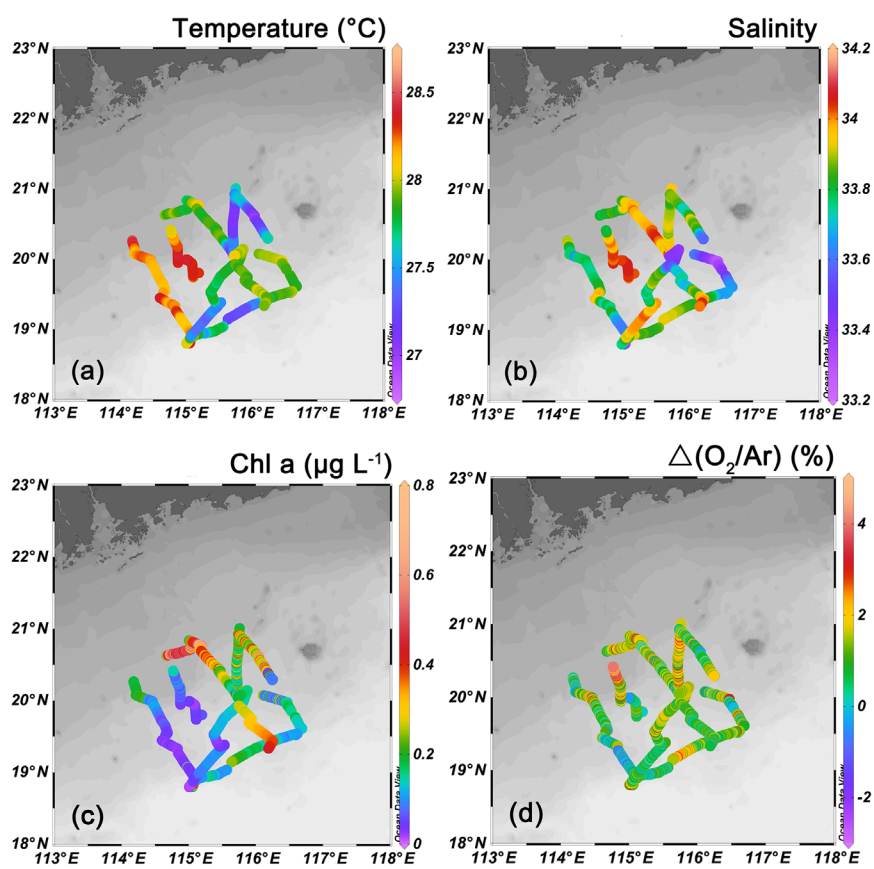


Figure 2. Surface distributions of (a) temperature, (b) salinity, (c) chlorophyll-a (Chl a), and (d) $\Delta(\text{O}_2/\text{Ar})$ in October 2014

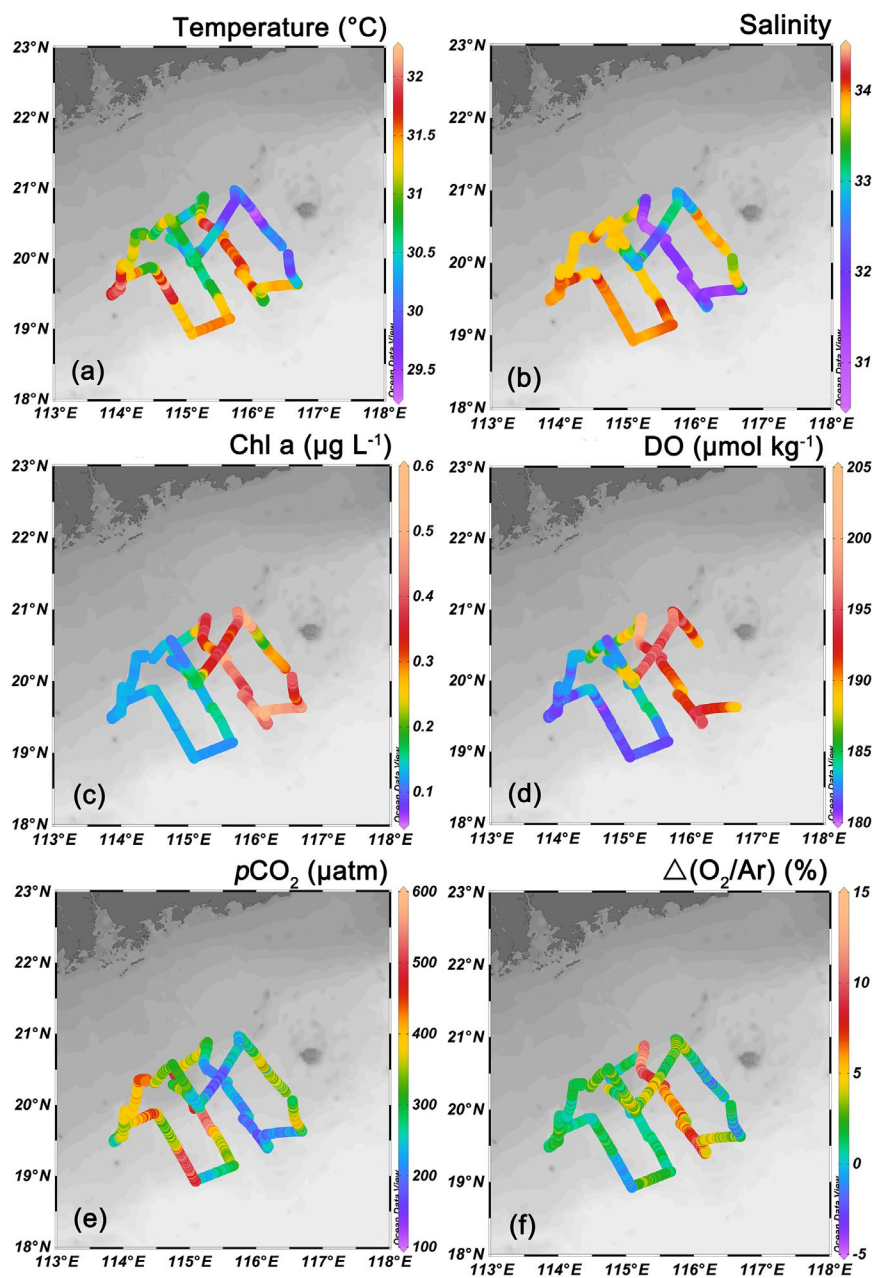


Figure 3. Surface distributions of (a) temperature, (b) salinity, (c) chlorophyll-a (Chl a), (d) dissolved oxygen (DO), (e) $p\text{CO}_2$, and (f) $\Delta(\text{O}_2/\text{Ar})$ in June 2015

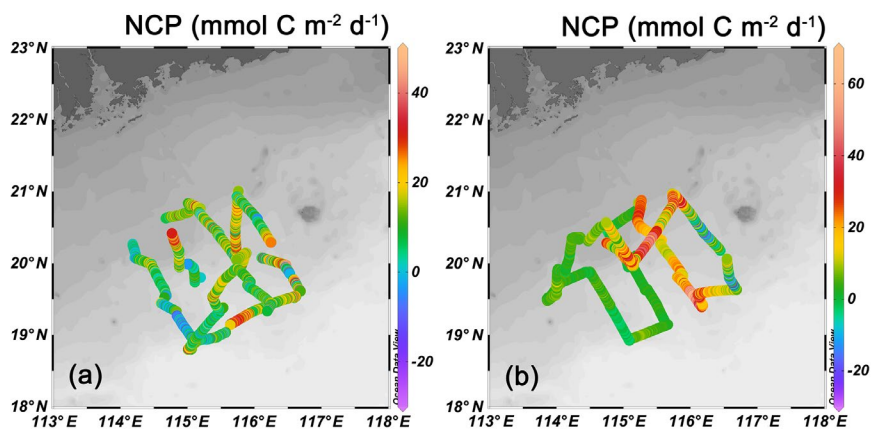


Figure 4. Surface distribution of NCP along the northern slope of SCS during the cruise in (a) October 2014 and (b) June 2015.

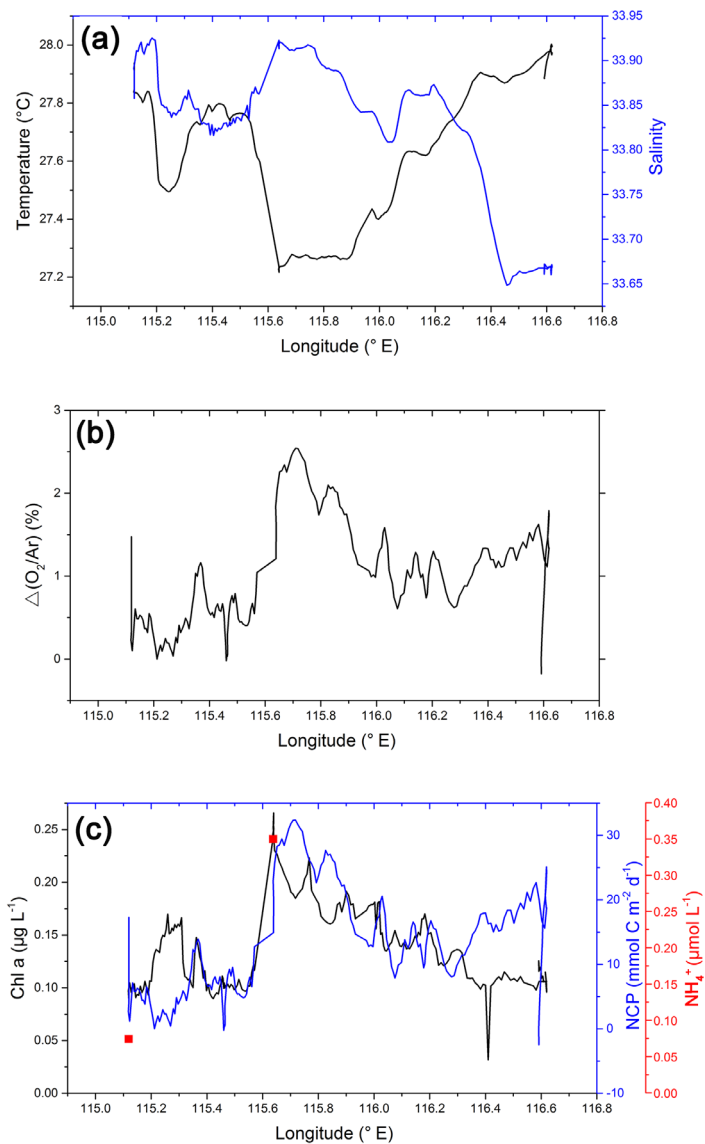


Figure 5. Zonal variations in (a) temperature, salinity, (b) $\Delta(O_2/Ar)$, (c) Chl a, NCP and surface concentration of ammonia (NH_4^+) along Transect 5 in October 2014. The plots of $\Delta(O_2/Ar)$ and NCP are 10-point Savitzky-Golay smoothed to give a better view of their distribution.

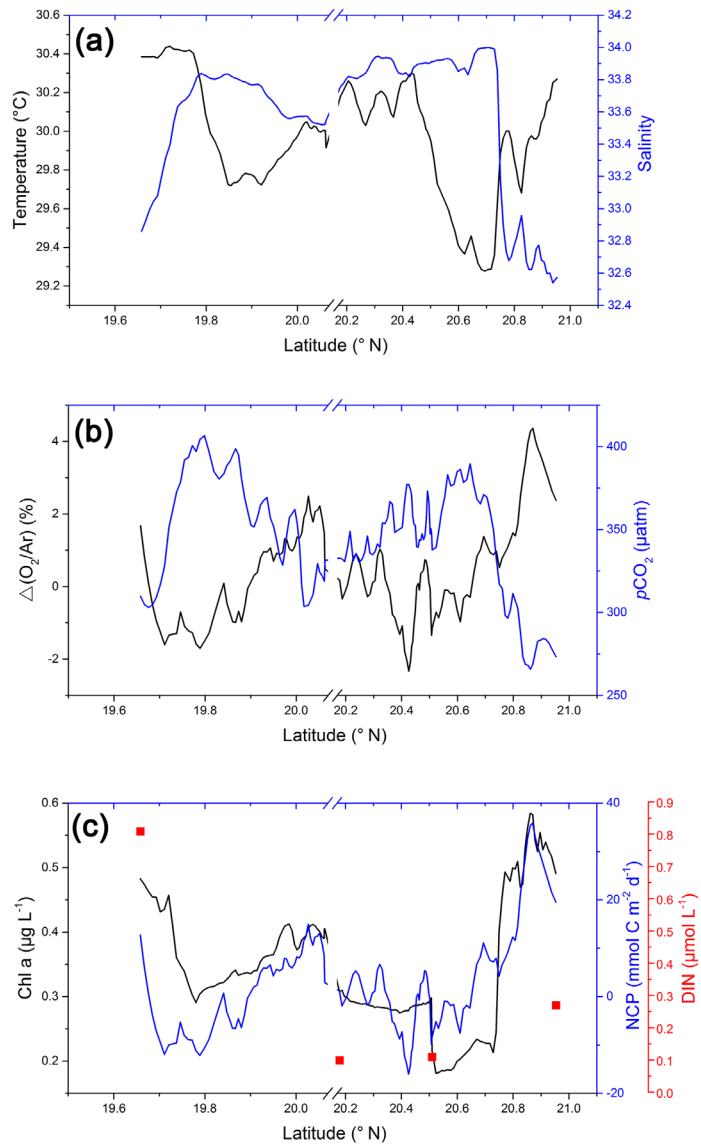


Figure 6. Meridional variations in (a) temperature, salinity, (b) $\Delta(O_2/Ar)$, pCO_2 , (c) Chl a, NCP and surface concentration of DIN along Transect 4 in June 2015. The plots of $\Delta(O_2/Ar)$, pCO_2 and NCP are 10-point Savitzky-Golay smoothed.

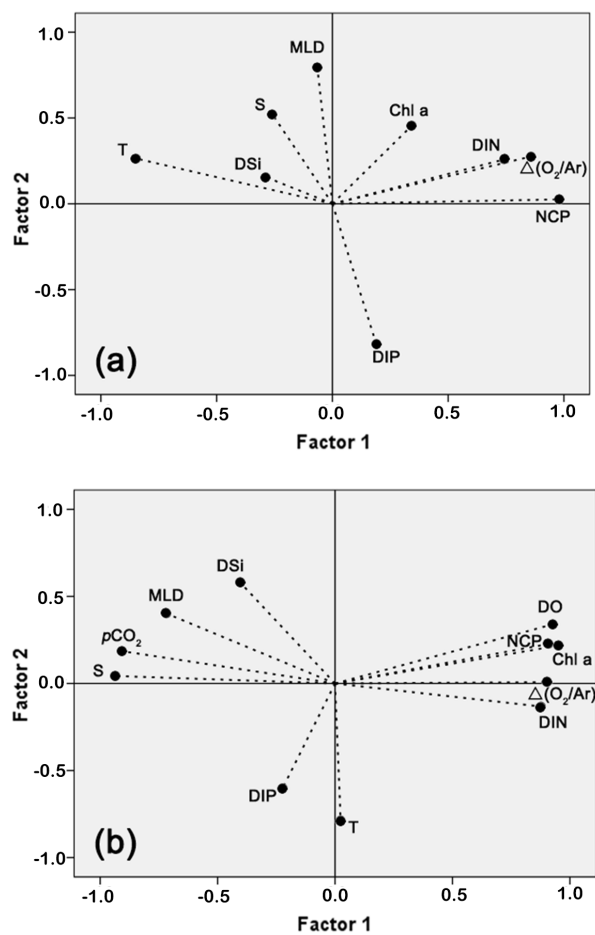


Figure 7. Principal Component Analysis (PCA) among variables for (a) October 2014 and (b) June 2015 (Bartlett's test of sphericity: $p < 0.01$)

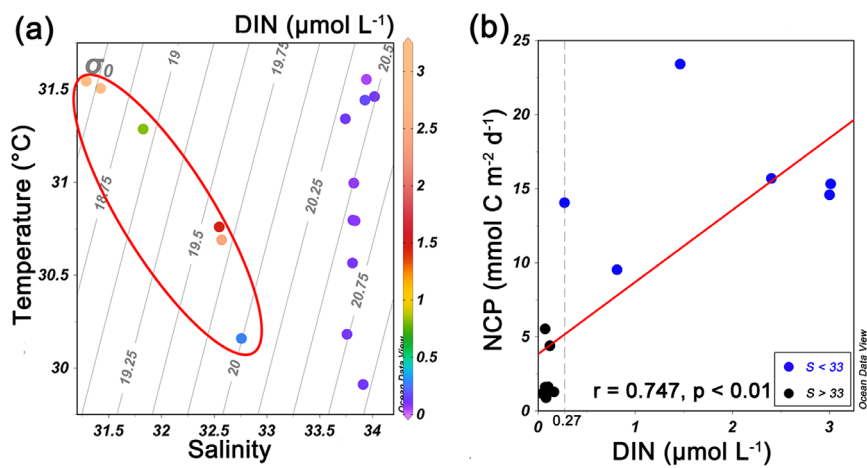


Figure 8. (a) T-S diagram of surface DIN concentration in June 2015. The stations influenced by shelf water were in the red circle. (b) Correlation analysis between surface DIN concentration and NCP at sampling stations. The stations (characterized with $S < 33$) influenced by shelf water presented surface DIN concentration $\geq 0.27 \mu\text{mol L}^{-1}$.

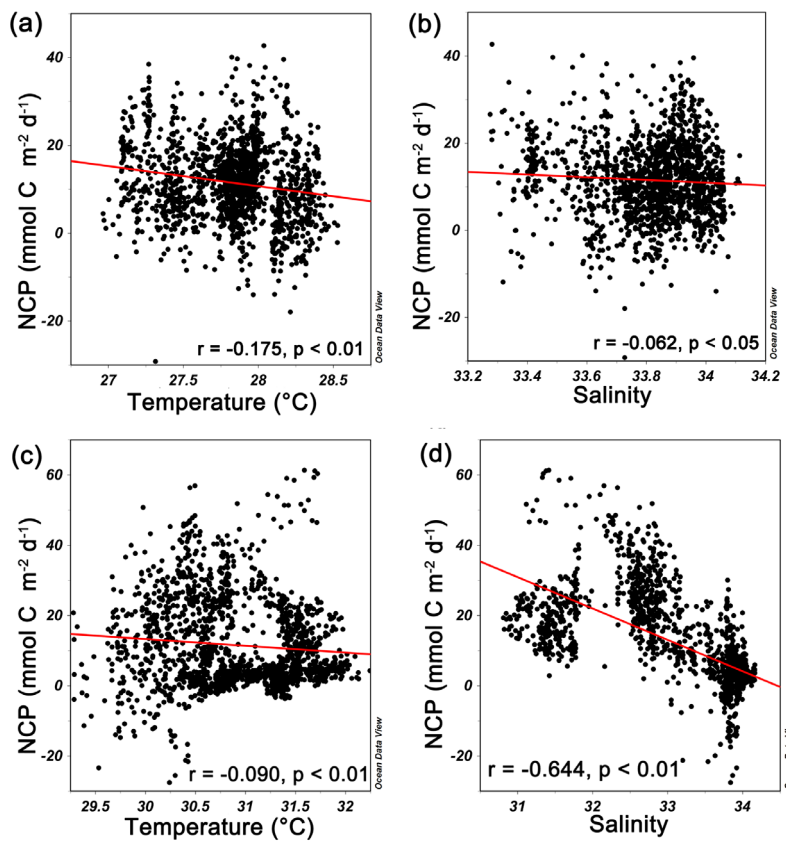


Figure 9. Correlation analysis between undersea NCP and physical parameters (temperature and salinity) in October 2014 (a, b) and June 2015 (c, d).

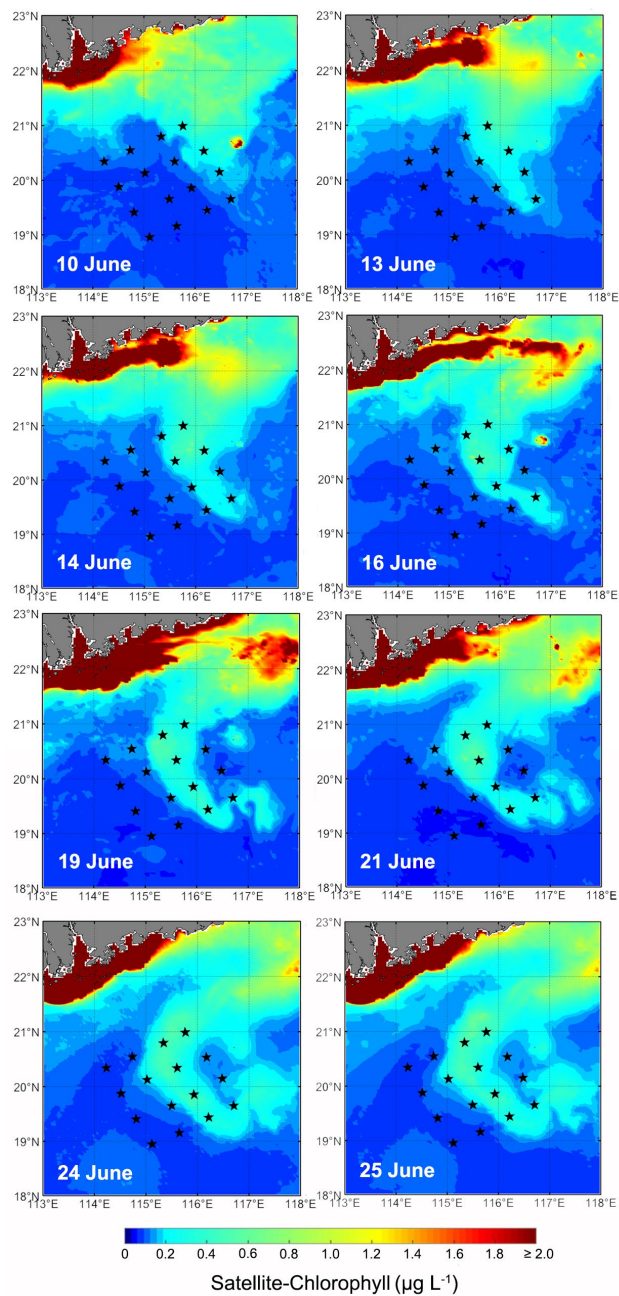


Figure 10. Daily satellite-chlorophyll images on the selected days in June 2015. Stars represent CTD locations. We roughly set satellite-chlorophyll $\geq 0.2 \mu\text{g L}^{-1}$ in this figure as the criterion of shelf water. This figure was made based on the M_Map mapping package for MATLAB (Pawlowicz, 2020).

Supplementary

Table S1a. Correlation coefficient matrix of PCA in October 2014										
		Temperature (T)	Salinity (S)	DIN	DIP	DSi	MLD	Chl a	$\Delta(\text{O}_2/\text{Ar})$	NCP
Correlation coefficient	Temperature (T)	1.000	0.190	−0.536	−0.305	0.539	0.267	−0.162	−0.524	−0.757
	Salinity (S)	0.190	1.000	0.098	−0.337	−0.492	0.352	0.145	−0.295	−0.359
	DIN	−0.536	0.098	1.000	0.000	−0.132	0.176	0.125	0.574	0.706
	DIP	−0.305	−0.337	0.000	1.000	−0.264	−0.494	−0.267	−0.075	0.135
	DSi	0.539	−0.492	−0.132	−0.264	1.000	0.098	0.051	−0.024	−0.171
	MLD	0.267	0.352	0.176	−0.494	0.098	1.000	0.068	0.202	−0.037
	Chl a	−0.162	0.145	0.125	−0.267	0.051	0.068	1.000	0.397	0.323
	$\Delta(\text{O}_2/\text{Ar})$	−0.524	−0.295	0.574	−0.075	−0.024	0.202	0.397	1.000	0.906
	NCP	−0.757	−0.359	0.706	0.135	−0.171	−0.037	0.323	0.906	1.000
Statistical significance	Temperature (T)		0.288	0.044	0.181	0.043	0.214	0.317	0.049	0.003
	Salinity (S)			0.388	0.155	0.062	0.144	0.335	0.189	0.139
	DIN		0.044	0.388	0.500	0.350	0.302	0.358	0.032	0.008
	DIP		0.181	0.155	0.500	0.216	0.061	0.214	0.413	0.346
	DSi		0.043	0.062	0.350	0.216	0.387	0.441	0.473	0.307
	MLD		0.214	0.144	0.302	0.061	0.387	0.422	0.275	0.457
	Chl a		0.317	0.335	0.358	0.214	0.441	0.422	0.113	0.167
	$\Delta(\text{O}_2/\text{Ar})$		0.049	0.189	0.032	0.413	0.473	0.275	0.113	0.000
	NCP		0.003	0.139	0.008	0.346	0.307	0.457	0.167	0.000

074

Table S1b. Component matrix of variables in
October 2014

	Factor 1	Factor 2
Temperature (T)	−0.847	0.264
Salinity (S)	−0.259	0.521
DIN	0.741	0.259
DIP	0.189	−0.817
DSi	−0.288	0.156
MLD	−0.065	0.793
Chl a	0.343	0.456
$\Delta(\text{O}_2/\text{Ar})$	0.858	0.276
NCP	0.979	0.026

075

076

077

Table S2a. Correlation coefficient matrix of PCA in June 2015

	Temperature (T)	Salinity (S)	DIN	DIP	DSi	MLD	Chl a	pCO ₂	DO	Δ(O ₂ /Ar)	NCP	
Correlation coefficient	Temperature (T)	1.000	−0.128	0.217	0.150	−0.239	−0.244	−0.156	−0.189	−0.313	0.060	−0.224
	Salinity (S)	−0.128	1.000	−0.873	0.163	0.301	0.614	−0.921	0.859	−0.831	−0.816	−0.787
	DIN	0.217	−0.873	1.000	−0.067	−0.260	−0.594	0.754	−0.705	0.736	0.910	0.747
	DIP	0.150	0.163	−0.067	1.000	−0.222	−0.017	−0.349	0.165	−0.355	−0.172	−0.195
	DSi	−0.239	0.301	−0.260	−0.222	1.000	0.474	−0.275	0.443	−0.241	−0.361	−0.276
	MLD	−0.244	0.614	−0.594	−0.017	0.474	1.000	−0.593	0.816	−0.541	−0.507	−0.518
	Chl a	−0.156	−0.912	0.754	−0.349	−0.275	−0.593	1.000	−0.867	0.948	0.793	0.884
	pCO ₂	−0.189	0.859	−0.705	0.165	0.443	0.816	−0.867	1.000	−0.762	−0.701	−0.767
	DO	−0.313	−0.831	0.736	−0.355	−0.241	−0.541	0.948	−0.762	1.000	0.839	0.946
	Δ(O ₂ /Ar)	0.060	−0.816	0.910	−0.172	−0.361	−0.507	0.793	−0.701	0.839	1.000	0.846
	NCP	−0.224	−0.787	0.747	−0.195	−0.276	−0.518	0.884	−0.767	0.946	0.846	1.000
Statistical significance	Temperature (T)		0.331	0.228	0.305	0.205	0.200	0.297	0.259	0.138	0.420	0.220
	Salinity (S)	0.331		0.000	0.288	0.148	0.010	0.000	0.000	0.000	0.000	0.000
	DIN	0.228	0.000		0.410	0.185	0.013	0.001	0.002	0.001	0.000	0.001
	DIP	0.305	0.288	0.410		0.223	0.477	0.111	0.286	0.106	0.279	0.252
	DSi	0.205	0.148	0.185	0.223		0.043	0.170	0.056	0.203	0.102	0.170
	MLD	0.200	0.010	0.013	0.477	0.043		0.013	0.000	0.023	0.032	0.029
	Chl a	0.297	0.000	0.001	0.111	0.170	0.013		0.000	0.000	0.000	0.000
	pCO ₂	0.259	0.000	0.002	0.286	0.056	0.000	0.000		0.001	0.003	0.001
	DO	0.138	0.000	0.001	0.106	0.203	0.023	0.000	0.001		0.000	0.000
	Δ(O ₂ /Ar)	0.420	0.000	0.000	0.279	0.102	0.032	0.000	0.003	0.000		0.000
	NCP	0.220	0.000	0.001	0.252	0.170	0.029	0.000	0.001	0.000	0.000	

1081

Table S2b. Component matrix of variables
in June 2015

	Factor 1	Factor 2
Temperature (T)	0.024	−0.786
Salinity (S)	−0.936	0.043
DIN	0.876	−0.132
DIP	−0.223	−0.601
DSi	−0.405	0.582
MLD	−0.718	0.402
Chl a	0.950	0.217
pCO ₂	−0.908	0.186
DO	0.927	0.340
Δ(O ₂ /Ar)	0.902	0.008
NCP	0.909	0.227

1082

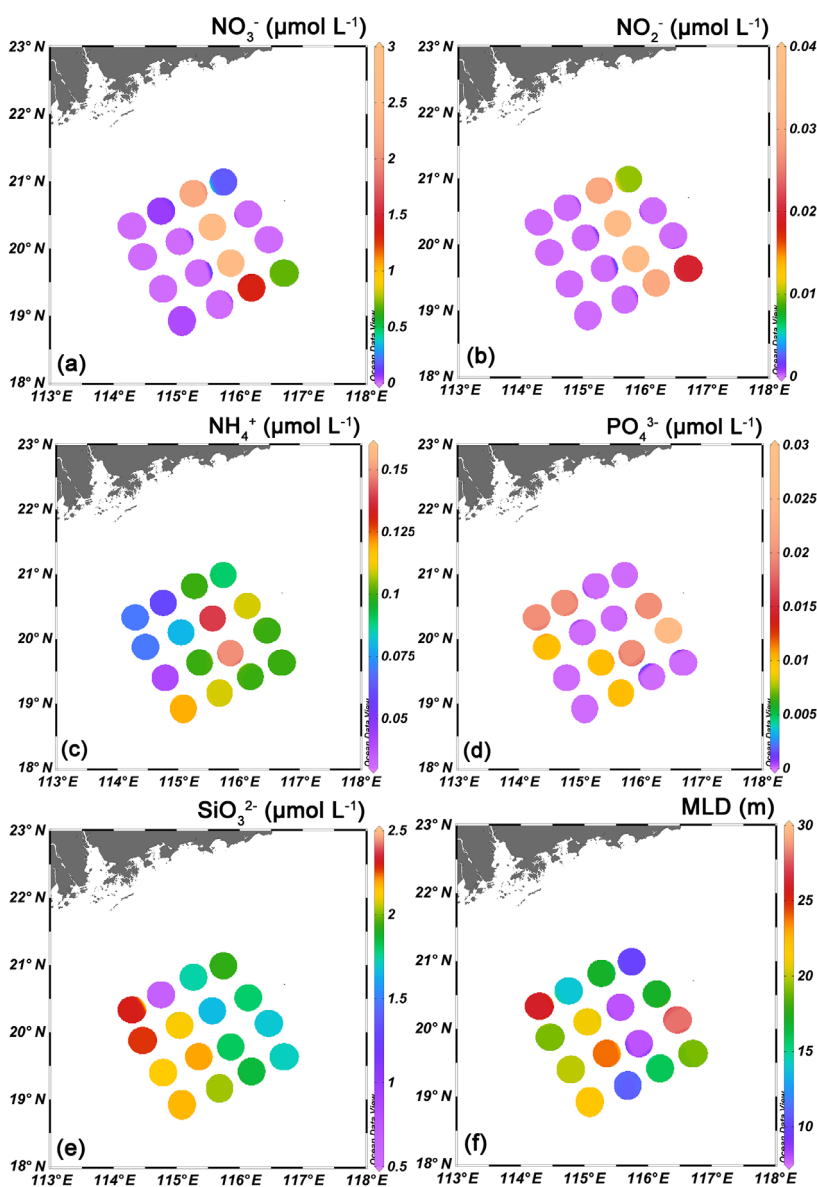


Figure S1. Surface distributions of (a) nitrate (NO_3^-), (b) nitrite (NO_2^-), (c) ammonium (NH_4^+), (d) phosphate (PO_4^{3-}), (e) silicate (SiO_3^{2-}) and (f) mixed layer depth (MLD) in June 2015. We regarded the nutrients data that were below the detection limit as “0” when made these plots.

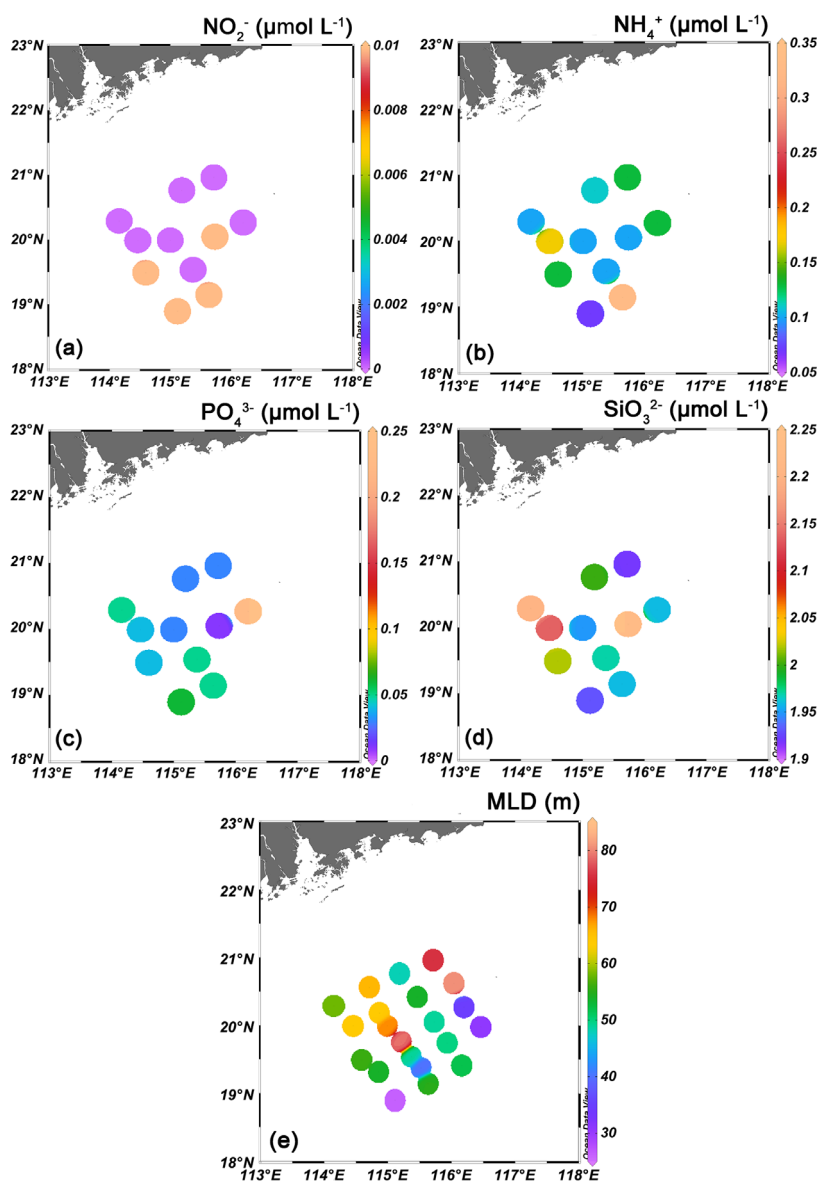


Figure S2. Surface distributions of (a) nitrite (NO_2^-), (b) ammonium (NH_4^+), (c) phosphate (PO_4^{3-}), (d) silicate (SiO_3^{2-}) and (e) mixed layer depth (MLD) in October 2014. The surface concentration of nitrate (NO_3^-) at all sampling stations was below the detection limit during this cruise. We regarded the nutrients data that were below the detection limit as “0” when made these plots.